Original Article
In-silico analysis of TMEM2 as a pancreatic adenocarcinoma and cancer-associated fibroblast biomarker, and functional characterization of NSC777201, for targeted drug development

Prateeti Srivastava[1,2], Vijesh Kumar Yadav[3,4], Tzu-Hao Chang[2,5], Emily Chia-Yu Su[2], Bashir Lawal[6,7], Alexander TH Wu[1,2,8,9,10,11], Hsu-Shan Huang[8,12,13,14,15]

[1]The Program for Translational Medicine, Graduate Institute of Biomedical Informatics, College of Medical Science and Technology, Taipei Medical University, Taipei 110, Taiwan; [2]Graduate Institute of Biomedical Informatics, College of Medical Science and Technology, Taipei Medical University, Taipei 110, Taiwan; [3]Division of Gastroenterology and Hepatology, Department of Internal Medicine, Shuang Ho Hospital, New Taipei 23561, Taiwan; [4]Division of Gastroenterology and Hepatology, Department of Internal Medicine, School of Medicine, College of Medicine, Taipei Medical University, Taipei 110, Taiwan; [5]Clinical Big Data Research Center, Taipei Medical University Hospital, Taipei 110, Taiwan; [6]UPMC Hillman Cancer Center, University of Pittsburgh, Pittsburgh, PA 15232, USA; [7]Department of Pathology, University of Pittsburgh, Pittsburgh, PA 15213, USA; [8]Graduate Institute of Medical Sciences, National Defense Medical Center, Taipei 114, Taiwan; [9]The PhD Program for Translational Medicine, College of Medical Science and Technology, Taipei Medical University, Taipei 110, Taiwan; [10]TMU Research Center of Cancer Translational Medicine, Taipei Medical University, Taipei 110, Taiwan; [11]Clinical Research Center, Taipei Medical University Hospital, Taipei Medical University, Taipei 11031, Taiwan; [12]Graduate Institute for Cancer Biology and Drug Discovery, College of Medical Science and Technology, Taipei Medical University, Taipei 110, Taiwan; [13]PhD Program for Cancer Molecular Biology and Drug Discovery, College of Medical Science and Technology, Taipei Medical University, Academia Sinica, Taipei 11031, Taiwan; [14]School of Pharmacy, National Defense Medical Center, Taipei 11490, Taiwan; [15]PhD Program in Drug Discovery and Development Industry, College of Pharmacy, Taipei Medical University, Taipei 11031, Taiwan

Abstract: Pancreatic adenocarcinoma (PAAD), known as one of the deadliest cancers, is characterized by a complex tumor microenvironment, primarily comprised of cancer-associated fibroblasts (CAFs) in the extracellular matrix. These CAFs significantly alter the matrix by interacting with hyaluronic acid (HA) and the enzyme hyaluronidase, which degrades HA - an essential process for cancer progression and spread. Despite the critical role of this interaction, the specific functions of CAFs and hyaluronidase in PAAD development are not fully understood. Our study investigates this interaction and assesses NSC777201, a new anti-cancer compound targeting hyaluronidase. This research utilized computational methods to analyze gene expression data from the Gene Expression Omnibus (GEO) database, specifically GSE172096, comparing gene expression profiles of cancer-associated and normal fibroblasts. We conducted in-house sequencing of pancreatic cancer cells treated with NSC777201 to identify differentially expressed genes (DEGs) and performed functional enrichment and pathway analysis. The identified DEGs were further validated using the TCGA-PAAD and Human Protein Atlas (HPA) databases for their diagnostic, prognostic, and survival implications, accompanied by Ingenuity Pathway Analysis (IPA) and molecular docking of NSC777201, *in-vitro*, and preclinical *in-vivo* validations. The result revealed 416 DEGs associated with CAFs and 570 DEGs related to NSC777201 treatment, with nine overlapping DEGs. A key finding was the transmembrane protein TMEM2, which strongly correlated with FAP, a CAF marker, and was associated with higher-risk groups in PAAD. NSC777201 treatment showed inhibition of TMEM2, validated by rescue assay, indicating the importance of targeting TMEM2. Further analyses, including IPA, demonstrated that NSC777201 regulates CAF cell senescence, enhancing its therapeutic potential. Both *in-vitro* and *in-vivo* studies confirmed the inhibitory effect of NSC777201 on TMEM2 expression, reinforcing its role in targeting PAAD. Therefore, TMEM2 has been identified as a theragnostic biomarker in PAAD, influenced by CAF activity and HA accumulation. NSC777201 exhibits significant potential in

targeting and potentially reversing critical processes in PAAD progression, demonstrating its efficacy as a promising therapeutic agent.

Introduction

Pancreatic cancer (PC) is one of the most aggressive and deadliest malignant neoplasms worldwide, resulting from the abnormal and uncontrolled growth of cells in the pancreatic tissue. It is the second leading cause of mortality among malignant cancer-associated diseases [1, 2]. Pancreatic adenocarcinoma (PAAD), the commonest form of PC, accounts for approximately 85% of all types of PC and is connected with a poor prognosis [3].

Treatment approaches for PC include surgical resection, radiotherapy, chemotherapy, neoadjuvant therapy, immunology, and targeted molecular therapy, alone or in combination [4]. Overall 5-year survival rates of PC are 34% when cancer remains local and grows in the pancreas, 12% when cancer has spread to nearby lymph tissues and 3% when cancer has metastasized to other organs and lymph nodes [5]. PC has a higher recurrence rate and lower disease-free survival (DFS) even in patients receiving adjuvant chemotherapy after surgical resection [6]. As the overall survival (OS) rate of patients with early tumor recurrence is significantly lower than those of patients without early tumor recurrence [7], it is important to discover novel strategies for predicting recurrence.

Recent studies have shifted focus towards the tumor microenvironment (TME) of pancreatic adenocarcinoma (PAAD), underscoring its complexity with a composition of inflammatory cells, fibroblasts, immune cells, and growth factors within the extracellular matrix (ECM). This dense stromal tissue, accounting for 15% to 85% of the entire tumor component of PAAD [8, 9], plays a pivotal role in tumor proliferation, invasion, and the ability to metastasize, largely influenced by the ECM remodelling by fibroblasts [10]. Cancer-associated fibroblasts (CAFs) within the ECM, crucial for promoting tumor progression and chemoresistance, release growth factors and cytokines that stimulate tumor growth and metastasis [11-14], also contributing to the poor prognosis of PAAD

by fostering an immunosuppressive environment [15-18]. With a deeper understanding of the TME of PC, TME-based translational therapies may be a breakthrough in future PC treatments. Hyaluronic acid (HA), a major ECM component, crucial in many cancers [19-21], influences cell adhesion, migration, and proliferation, and is associated with a malignant phenotype [22-28]. The degradation of HA by enzymes, including the novel hyaluronidase transmembrane protein 2 (TMEM2), also known as CEMIP2 (cell migration-inducing hyaluronidase 2), impacts a wide variety of cancers [29-35], with its role in PAAD still to be fully understood. Despite advancements in bioinformatics, the association of TMEM2 with the PAAD-TME, especially its interaction with CAFs, remains underexplored. Investigating TMEM2's role could unveil new therapeutic targets, potentially improving treatment outcomes for PAAD.

Our research previously identified a series of tetracyclic heterocyclic azathioxanthones with significant cytotoxic effects against cancer cells as multi-kinase inhibitors [36], noting the diversity of this representative scaffold of the small molecule [37-40]. In our ongoing study, we focus on evaluating the candidate, NSC777201's ability to target pancreatic adenocarcinoma (PAAD) by inhibiting the HA-enzyme, TMEM2, which we found to be overexpressed in PAAD through analysis of public GEO database gene expression profiles of cancer-associated fibroblasts (CAFs) and normal fibroblasts (NFs). Treatment with NSC777201 significantly decreased TMEM2 expression in Panc1 cells, a finding supported by data from The Cancer Genome Atlas (TCGA)-PAAD and the Human Protein Atlas (HPA), which revealed overexpression of TMEM2 at both mRNA and protein levels in pancreatic adenocarcinoma (PAAD) compared to normal tissue. Co-expression analysis revealed a strong association between TMEM2 and cancer-associated fibroblast (CAF) markers, particularly the fibroblast activation protein (FAP). Ingenuity Pathway Analysis (IPA) of cells treated with NSC777201 indicated a reduction

in fibroblast activity and an induction of senescence, highlighting the compound's effectiveness. This was further supported by *in silico* molecular docking, which demonstrated robust binding of NSC777201 to TMEM2. *In-vitro* assays and rescue experiments confirmed that NSC777201 specifically targets TMEM2. This targeting efficacy was also reinforced by pre-clinical *in-vivo* studies using a mouse model, confirming NSC777201's potential to alter the PAAD tumor microenvironment (TME) by inhibiting TMEM2 and modulating CAF activity, ultimately reducing tumor growth. These results underscore the potential of NSC777201 as a promising therapeutic candidate for PAAD, warranting further development.

Materials and methods

Acquisition of RNA expression dataset

RNA expression data from GSE172096, including five CAF and three NF samples derived from human pancreatic ductal adenocarcinoma, were downloaded from the publicly available GEO database (http://www.ncbi.nlm.nih.gov/geo/). For further validation, the RNA-sequencing raw counts, and clinical data of patients with a pancreatic tumor (PAAD) and normal samples (n=178) were downloaded from TCGA (https://portal.gdc.cancer.gov/) database, stored, and used. Furthermore, online analysis databases, which use TCGA data, such as (a) http://gdac.broadinstitute.org/, (b) http://gepia.cancer-pku.cn/, and (c) http://ualcan.path.uab.edu/cgi-bin/ualcan-res.pl, were used for analysis and visualization of key genes.

Identification of DEGs

Expression raw data and annotation matrix were downloaded from the GEO database, the circular(circ) RNA IDs were correlated and matched with parent genes, circRNA and parental genes were closely associated. The expression data in the expression matrix were analyzed with DESeq2, an R package [41], a Bioconductor package for differentially expressed genes (DEGs) analysis of expression data, to determine the DEGs in between CAFs and NFs dataset, the criteria of |log2fold change| >1.25 and the adjusted *p* values of <0.05 were used. With thousands of genes tested, multiple comparison adjustments were necessary so, the Bonferroni method was applied for filtering

DEGs; this controls the mean number of false positives, that can be used for multiplicity adjustment [42]. Hierarchical clustering with a heatmap and a principal component analysis (PCA) were respectively generated using Heatmap.2 and the scatterplot3d function tool in R package gplots [43].

GO enrichment and kyoto encyclopedia of genes and genomes (KEGG) analysis of DEGs

GO, KEGG pathway, and cnet plot enrichment analyses were performed for CAF- vs. NF-identified DEGs using clusterProfiler, an R package [44].

Cell culture and reagents

The human pancreatic cancer cell line, PANC1 and SUIT2 was obtained from the American Type Culture Collection (ATCC; Manassas, VA, USA). The cell line was cultured in Dulbecco's modified Eagle medium (#12491023; GIBCO, Life Technologies Corp., Carlsbad, CA, USA) supplemented with 10% heat-inactivated fetal bovine serum (FBS) and antibiotics (100 μg/ml streptomycin and 100 IU/ml penicillin) at 37°C in a 5% CO_2 incubator. To maintain the cell lines, subcultures were performed every 48~72 hrs for maintenance. NSC777201 is one of our in-house drugs synthesized as previously described in a US patent application (H.S. Huang, D.S. Yu, T.C. Chen, Vol. US Patent No. 8,927,717B1, US, Jan. 6, 2015) [36]. For a stock solution, NSC777201 was dissolved in 10 mM dimethyl sulfoxide (DMSO; Sigma Aldrich, St. Louis, MO, USA) and kept at -20°C. The stock solution was further immediately diluted in a sterile medium to the required concentrations.

Sulforhodamine B (SRB) assay

PC cells (PANC1 and SUIT2) were seeded in 96-well plates (at 3000 cells/well). After the cells had attached to the plate (by 24 h of incubation), cells were randomly divided into control and treatment groups. The control group was treated with DMSO, while the treatment groups were treated with different doses of NSC777201. After 48 h of incubation, the medium was removed, and 100 μL 10% trichloroacetic acid (TCA) was added to each well. After incubation for 1 h at 4°C, TCA was removed, and 100 μL of the SRB reagent was

added to each well followed by incubation for 1 h at room temperature. All plates were washed with 1% acetic acid. After the plates were dried in an oven for 20 min at 60°C, 200 µL of Tris (20 nM) was added to each well. The absorbance was measured using spectrophotometry (at a wavelength of 565 nm). Absorbance values are reported as percent (%) cell viability (of treatment groups relative to the control group).

Tumor sphere-formation assay

The tumor sphere-formation assay was performed according to a previously described method with modifications. In short, PC cells (PANC1 and SUIT2) were seeded (2500 cells/ well) in six-well ultra-low attachment plates (Corning, Corning, NY, USA) in serum-free media consisting of Dulbecco's modified Eagle medium (DMEM)/Ham's F12 (1:1), human epidermal growth factor (hEGF, 20 ng/ml), basic fibroblast growth factor (bFGF; 10 ng/ml (PeproTech, Rocky Hill, NJ, USA), 2 µg/ml 0.2% heparin (Sigma, St. Louis, MO, USA), and 1% penicillin/streptomycin (P/S, 100 U/ml, Hyclone, Logan, UT, USA)). Cells were then allowed to aggregate and grow for at least 7 days. Cells (diameter >50 µm), characterized by compact, non-adherent spheroid-like masses, were considered a tumor-sphere and counted with an inverted phase-contrast microscope.

Wound-healing migration assay

PC cells were resuspended in a complete medium, plated in individual culture-inserts (ibdi, Munich, Germany), appropriated for a 2D migration assay, and maintained at 37°C in a 5% CO_2 atmosphere until confluence. These culture inserts were composed of two chambers separated by a biocompatible silicone material, which after removal allowed cells from each edge to migrate towards the center of the gap. After the barrier was removed, confluent cancer cell monolayers were washed with PBS to remove non-adherent cells and treated with NSC777201. Treated and untreated cells were maintained at 37°C in a 5% CO_2 atmosphere for 24 h. Cell migration was evaluated every 2 h with the BioTek Lionheart FX automated cell imaging system to capture and monitor wound closure with a phase-contrast microscope.

Gene expression sequencing and siRNA knock-down analysis

After NSC777201 treatment, Panc1 cells were collected in TRIzol reagent, and total RNA was isolated and purified using a TRIzol-based protocol (Life Technologies, USA) as per the manufacturer's instructions. The RNA concentration and purity were determined with a NanoDrop 1000 spectrophotometer (Nyxor Biotech, Paris, France). Two micrograms of total RNA were sent to Welgen Biotech Taiwan (New Taipei City, Taiwan; https://www.welgene.com.tw/main) for sequencing. The experimental flow for sequencing is illustrated in Figure S1. Analysis was performed as raw intensity with background correction, then quantile normalized intensity between samples done, for differential expression analysis between treated and control samples, was analyzed with limma, an R package, a Bioconductor packages for differentially expressed genes (DEGs) analysis of expression data, to determine the DEGs in between NSC777201 treated and control dataset, the criteria of |log2fold change| >1.2 was applied. Furthermore, for RT-PCR analysis, one microgram of total RNA was reverse-transcribed using a Qiagen OneStep RT-PCR Kit (Qiagen), and the PCR was performed using a Rotor-Gene SYBR Green PCR Kit (400, Qiagen). Details of qPCR primers used for this study are listed in Table S1. siRNA-mediated mRNA knockdown, a population of 1 × 10*6 PC cells was cultured on a 10 cm plate. On the following day, siRNAs specifically aimed at TMEM2 (sourced from Integrated DNA Technologies (IDT), siRNA#1, and siRNA#2) were introduced into the cells along with a control siRNA (procured from Thermo Scientific; Control siRNA). This was completed using the Lipofectamine reagent, adhering strictly to the guidelines provided by the manufacturer. After allowing 48 hours post-transfection for the process to take effect, the cells were harvested.

For TMEM2 stable and longer expression a construction of TMEM2 Overexpression and Silencing Vectors, and Transfection Procedures, a TMEM2 overexpression (TMEM2-OE) vector was created by inserting the TMEM2 coding sequence into the pcDNA3.1+ vector. For shRNA-mediated TMEM2 silencing, the specific shRNA sequence (shTMEM2: GTGAGAAACTAT-GAAAATCATAG) was incorporated into the pLKO.1 vector (Genepharm). In overexpression

studies, Panc1 cells were cultured until they reached 70 to 90% confluency and then transfected with the TMEM2 overexpression vector using Lipofectamine 2000 reagent (Thermo Fisher Scientific) over 48 hours. For knockdown assays, Panc1 were grown to 80% confluency and transfected either with scramble shRNA (control) or shTMEM2 utilizing the same Lipofectamine 2000 reagent for 48 hours. Post-transfection, Overexpression and silencing of the TMEM2 gene in Panc1 cells were confirmed by quantitative RT-PCR and Western blotting, then the cells were collected and subsequently, these cells were utilized in various assays.

Sodium dodecyl sulfate-polyacrylamide gel electrophoresis (SDS-PAGE) and Western blot analysis

Total protein lysates from PC cells (parental, tumor-spheres, and transfected) were extracted after treatment in different experiments and were separated by SDS-PAGE using the Mini-Protean III system (Bio-Rad, Taiwan) and transferred onto polyvinylidene difluoride membranes using the Trans-Blot Turbo Transfer System (Bio-Rad). Membranes were incubated with the primary antibody to react overnight at 4°C. Details of the primary antibody and dilutions used for these studies are listed in Table S1. Then membranes were incubated with the horseradish peroxidase-labelled secondary antibody. Proteins of interest were detected and visualized using enhanced chemiluminescence (ECL) detection kits (ECL Kits; Amersham Life Science, NJ, USA). Images were captured and analyzed using the UVP BioDoc-It system (Upland, CA, USA).

Survival, risk score and diagnostic/prognostic significance of DEGs

Survival analysis and prognostic value of the messenger (m)RNA in the PAAD signature for both survival and risk between groups were analyzed using the online database SurvExpress (http://bioinformatica.mty.itesm.mx:8080/Biomatec/SurvivaX.jsp) [45]. High- and low-risk groups were divided by the risk score algorithm embedded in the platform. The pROC R package [46] was used to plot receiver operating characteristic (ROC) curves for key genes in PAAD, and values of the area under the curve (AUC) were calculated to assess their diagnostic values in PAAD.

The HPA: immunohistochemical (IHC) quantification, visualization, and subcellular localization

Expressions of key proteins and their correlations at the protein level were checked on the HPA (HPA; http://www.proteinatlas.org/) using the R package programs, hpar and HPAanalyze [47].

Ingenuity pathway analysis (IPA)

Ingenuity Pathway Analysis (IPA) was run to identify the canonical pathway network [48], accessed on 6th Nov 2021, it uses the popular activation z-score analytical method, as proposed by Kraèmer et al. in 2014 [48], which measures activation states (either increased or decreased) of pathways affected by the DEGs. We used a statistical method to define a quantitative z-score, which determines whether the biological function has been significantly more "increased" predictions than "decreased" predictions (z-score >0) or vice versa (z-score <0). In general practice, an absolute z-score of >2 or <-2 may be significant.

Molecular docking analysis

Studies were performed using the automated CB-Dock server (http://clab.labshare.cn/cb-dock/php/index.php; accessed on 10 November 2021) [49] with default parameters to investigate interactions between NSC777201 and TMEM2. The crystal structure of TMEM2 was not available; therefore, homologous modelling (comparative protein structure modelling) was used to find the three-dimensional (3D) structure of the TMEM2 protein obtained from the uniport database (https://www.uniprot.org/uniprot/Q9UHN6; accessed on 8 November 2021), and the NSC777201 3D structure was drawn in Sybyl mol2 using the Avogadro molecular builder and visualization tool vers. 1.1.0 [50]. Once the molecular docking experiments were completed and five configurations for each protein-ligand complex were generated for NSC777201 and TMEM2, the lowest binding affinity (kcal/mol) complex was considered to be the most stable docking pose. The interaction between the ligand and proteins was then prepared, visualized, and analyzed using the Discovery studio visualizer vers. 21.1.0.20298 (BIOVIA, San Diego, CA, USA) [51].

Animal studies

All the animal experiments and maintenance complied with the Animal Use Protocol at Taipei Medical University (protocol LAC-2017-0161). Five-week-old female NOD/SCID mice were purchased from BioLASCO (Taipei, Taiwan). The mice were maintained under pathogen-free conditions and were provided with sterilized food and water. Cells (1×10^6) were suspended in 0.2 mL serum-free DMEM and were injected subcutaneously into the right flank near the hind leg of each mouse. Tumor size was calculated using the formula V = width^2 × length/2. When the tumors became palpable (the tumor volume was ~100 mm^3), the mice were then randomly divided into three groups, i.e. control, sh-TMEM2 and NSC777201 (NSC777201, 10 mg/kg, five times/week) treated (only) group. The changes in the tumor volume, body weight (BW), and survival were monitored and recorded every week. The animals were humanely euthanized after the experiments were terminated, and the tumor samples were harvested for further analysis.

Statistical analysis

GraphPad Prism 8.0 (GraphPad Software, San Diego, CA, USA) was used to draw the figures. Pearson's Chi-squared test was used to compare categorical variables. The student's t-test was used to analyze the normal distribution of continuous variables. Kaplan-Meier (KM) plots with the log-rank test were used to estimate survival differences. The diagnostic significance of selected genes for PAAD was evaluated by the ROC curve. Statistical significance was indicated p or adjusted P<0.05.

Results

Identification of DEGs between PAAD-derived CAFs and NFs

To determine the gene expression patterns between PAAD-derived CAFs and NFs from the publicly available GEO database (GSE172096, n=8 total samples), details of sample and sequencing platform shown in Table S2, hierarchical clustering analysis of top genes was performed; data demonstrated that as shown in the heatmap, **Figure 1A**. Principal component analysis (PCA) was utilized to visualize the spatial distribution of the samples, which distin-

guishes CAF samples from NF samples (**Figure 1B**), In total, 416 DEGs were obtained, including 339 upregulated and 77 downregulated DEGs in CAFs vs. NFs, based on the cut-off criteria |log2FC| >1.25 and *p*-adj. <0.05, shown in the volcano and heatmap of **Figure 1C**, **1D**. The complete list of DEGs is available in Table S3, all DEGs were included in the further analysis. The identified DEGs in CAFs and NFs were further analyzed to identify the associated GO and KEGG pathways, using the "clusterProfiler" package [53]. The GO enrichment analysis classified the DEGs into three functional groups, including biological processes (BPs), cellular components (CCs), and molecular functions (MFs) (The Gene Ontology Consortium, 2018) [54]. As shown in Figure S2A-C. In the BP category, the top three most enriched terms were "DNA integrity checkpoint", "DNA replication", and "chromatin remodelling". In the CC category, the top three most enriched terms were "cell leading edge", "lamellipodium", and "microtubule end". In the MF category, the top three most enriched terms were "ATPase activity", "Ras GTPase binding", and "guanyl-nucleotide exchange factor activity". Moreover, as shown in Figure S2D, the top three most enriched terms in the KEGG analysis were "Pathways in cancer", "N-glycan biosynthesis", and "Protein processing in endoplasmic reticulum". The GO-all, as shown in Figure S2E "cnetplot", depicts linkages of genes and biological concepts as a network, with "positive regulation of transcription", "DNA-templated", "protein targeting to peroxisome", "peroxisomal matrix", and "ubiquitin-protein transferase" being key pathways demonstrating roles in PAAD.

Overview of DEGs modulated by NSC777201

Before NSC777201 treatment on Panc1 cells, we identified the novel potential of NSC777201, as a drug candidate, the online SwissADME algorithm developed by the Swiss Institute of Bioinformatics (http://www.swissadme.ch/index.php; assessed on 23rd January 2022) and ADMETlab 2.0 (https://admetmesh.scbdd.com/service/screening/molecule) was used to predict the PKs, drug-likeness, and adsorption, distribution, metabolism, excretion, and toxicity (ADMET) properties of NSC777201, as shown in Figure S3, the NSC77201 pass the criteria to belong as a drug candidate.

To further investigate changes in gene expressions associated with NSC777201 treatment
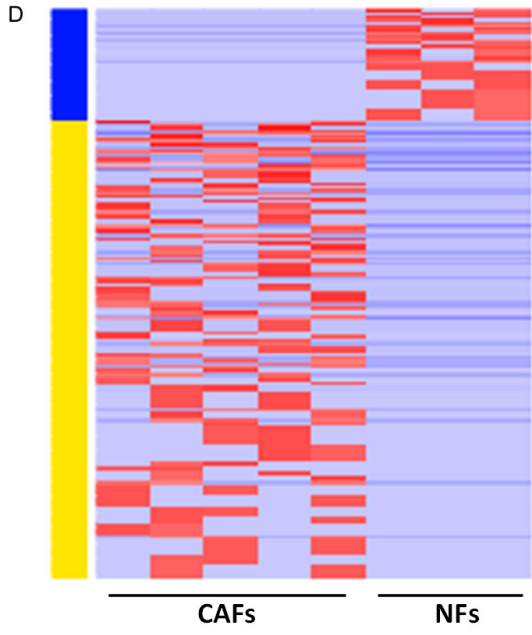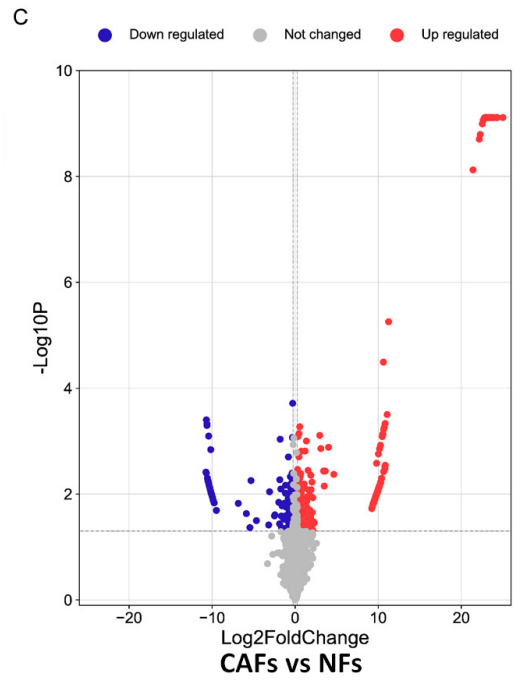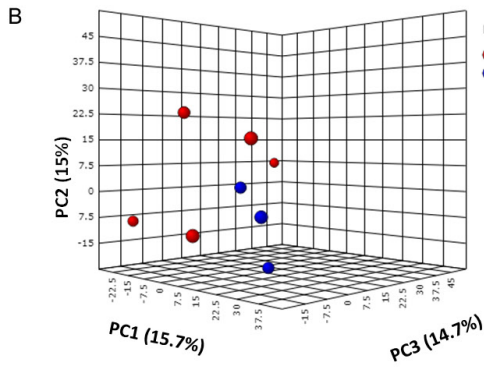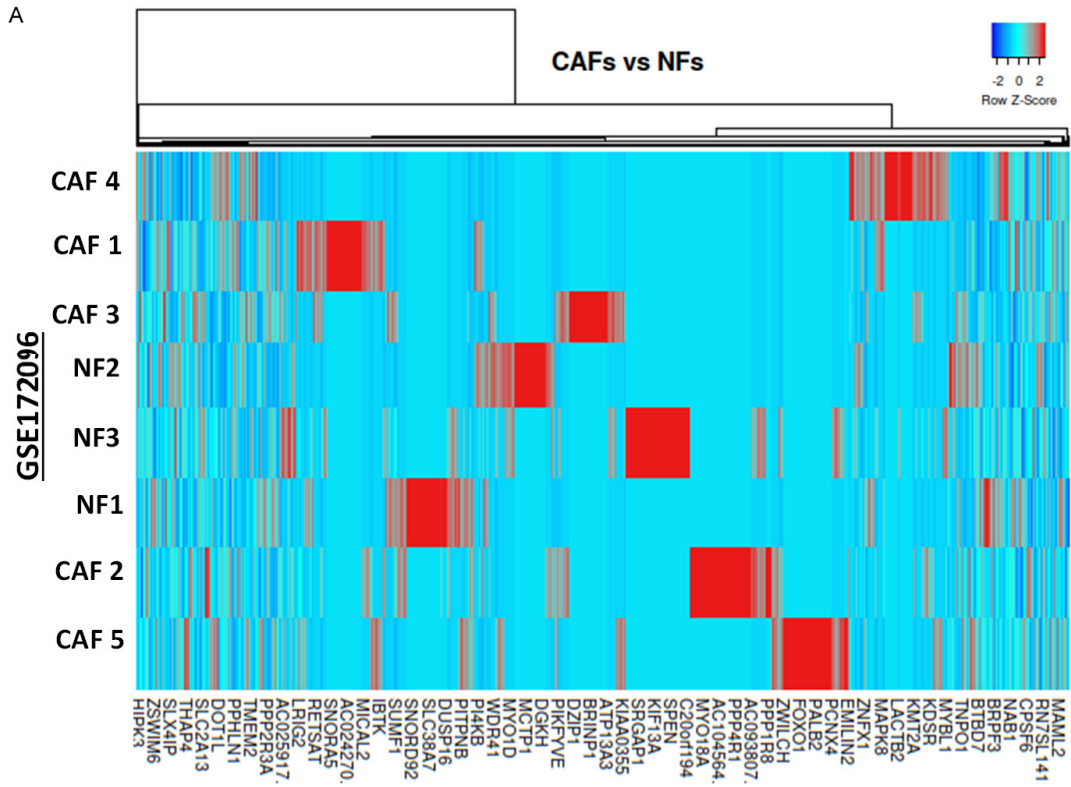
Figure 1. Identification of the candidate differentially expressed genes (DEGs) between cancer-associated fibroblasts (CAFs) and normal fibroblasts (NFs) samples. A. The expression heatmap and hierarchical clustering (n=8) of DEGs in GSE172096 datasets of human pancreatic ductal adenocarcinoma (PAAD). B. Principal component analysis (PCA). C, D. Volcano plot and heatmap in microarray representing top DEGs. DEGs are represented by satisfying the criteria of absolute log2fold changes (|log2FC|) value >1.25 and P<0.05.
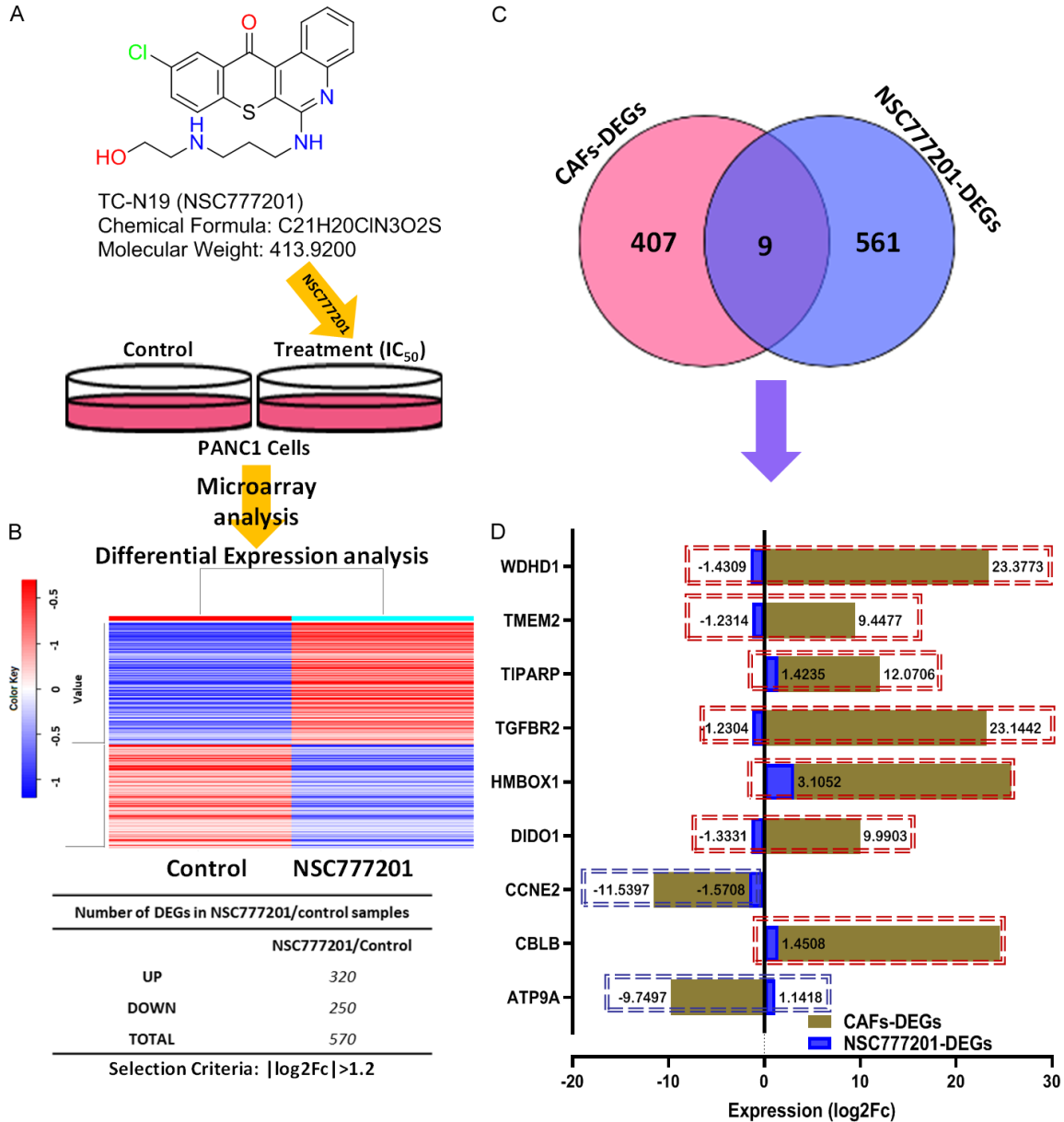
Figure 2. Microarray expression analysis of NSC777201 treated Panc1 cells. A. Molecular structure of NSC777201 and treatment of Panc1 cells. B. Heatmap displaying the DEGs between NSC777201-treated and control untreated cells. DEGs are represented by satisfying the criteria of |log2FC| >1.25. C. Venn diagram indicating overlapping DEGs between public dataset cancer-associated fibroblasts (CAFs) vs. normal fibroblasts (NFs) (GSE172096) and NSC777201-treated vs. untreated control cells. D. Horizontal bar graph showing the log2fold changes in expressions of nine common overlapping DEGs.

of Panc1 cells (**Figure 2A**), the percentage growth inhibition effect and 50% inhibitory con-

centration (IC50) values are shown in Figure S4, and microarray analysis was conducted for

a global gene expression pattern analysis (**Figure 2B**). In total, 570 DEGs were obtained, including 320 upregulated and 250 downregulated DEGs by applying the |log2FC| >1.2 criteria, as shown by a heatmap in **Figure 2B**, and a complete list of total NSC777201-related DEGs is shown in Table S4. Overlapping common genes between NSC777201-related DEGs and CAFs-DEGs are shown in a Venn diagram (**Figure 2C**), and a divergent stacked bar demonstrates nine DEGs that overlapped between NSC777201-related DEGs and CAFs-DEGs according to the fold change values (**Figure 2D**). These nine overlapping DEGs were used for further analyses.

Prognostic-related gene signatures of nine common overlapping DEGs

Expression levels of nine overlapping DEGs of both NSC777201-related DEGs and CAFs-DEGs are demonstrated in a heatmap in **Figure 3A**. Co-occurrence expressions of genes are often observed associated with functional inter-relatedness; therefore, we examined if and to what degree these nine overlapping DEGs were culpable in risk of death or recurrence in PAAD patients. We found that expression levels of these nine DEGs were equivocal as to the death risk, and higher expressions of these genes were strongly associated with a higher risk of death (**Figure 3B**). mRNA expression levels of these nine DEGs in the TCGA-PAAD (*n*=176) datasets by the risk group are shown in **Figure 3B**. In corroboration, a KM plot was generated for survival analysis of the co-expression of these nine DEG signatures in the TCGA-PAAD cohort (**Figure 3C**). Results showed that compared to the low-expression group, patients with higher expression levels of these nine DEGs exhibited worse mid-term to long-term (>5 years) OS ((hazard ratio (HR) =4.9), (95% confidence interval =2.14~11.21); *P*= 0.0001685). Moreover, to evaluate the prognostic model, the ROC curve analysis using the R survival timeROC, and pROC were used to generate the plot. Showed that this risk score model could contribute to determining the relationships of these nine DEGs with OS. AUCs for the time-dependent ROC curve are shown in **Figure 3D** for the nine DEGs. Furthermore, distributions of expression levels of these nine overlapping DEGs in the normal, tumor, and metastatic TCGA-PAAD samples are presented

in **Figure 3E**. Interestingly, CEMIP2 (TMEM2) was one of the DEGs significantly overexpressed in CAF vs. NF samples and TCGA-PAAD tumor and metastasis samples compared to normal samples, and it remains associated with the higher risk group in PAAD (**Figure 3A**, **3B**, **3D**, **3E**), and markedly significant suppression of TMEM2 was observed after NSC777201 treatment (**Figure 3A**). Therefore, we selected TMEM2 for further analysis and study.

TMEM2 mrna expression in PAAD

TCGA-PAAD data were used to verify the findings of this study. mRNA expression levels of TMEM2, pathological stage, and protein expressions in PC and normal tissues were analyzed. TMEM2 expression levels in 37 different cancer types are demonstrated in **Figure 4A**. Higher levels of TMEM were detected in PC tissues than in normal tissues (**Figure 4B**). Among PAAD patients, the relative expression level of TMEM2-mRNA was significantly higher in stage 4 patients than in stage 1 and normal patients (P<0.05; **Figure 4C**), and TMEM2 was significantly expressed in metastatic tumor than in normal samples (P=0.00000377; **Figure 4D**). Furthermore, the prognostic value of TMEM2 was examined using SurvExpress and kmplot (https://kmplot.com/analysis/). As shown in **Figure 4E**, we observed that patients with higher TMEM2 expression were associated with poorer OS compared to those with low TMEM2 expression levels (hazard ratio (HR) =31.64, 95% CI =1.06-2.52; log-rank P<0.023), and patients with higher expression levels of TMEM2 were strongly associated with a higher risk of death **Figure 4F** (left panel). mRNA expression levels of TMEM2 in TCGA-PAAD datasets are shown by a risk group optimization in **Figure 4F** (right panel), which suggests that TMEM2's ability to predict the progression and prognosis of PAAD patients is still largely elusive.

IHC analysis of TMEM2 expression in human

Furthermore, to investigate the expression and distribution of the TMEM2 protein in human PC samples, we retrieved and analyzed the IHC, immunofluorescent, and stained cell data from the HPA (http://www.proteinatlas.org/; accessed 15 November 2021) using the R packages *hpar* and *HPAanalyze*. The importance of these data is that they provide a detailed

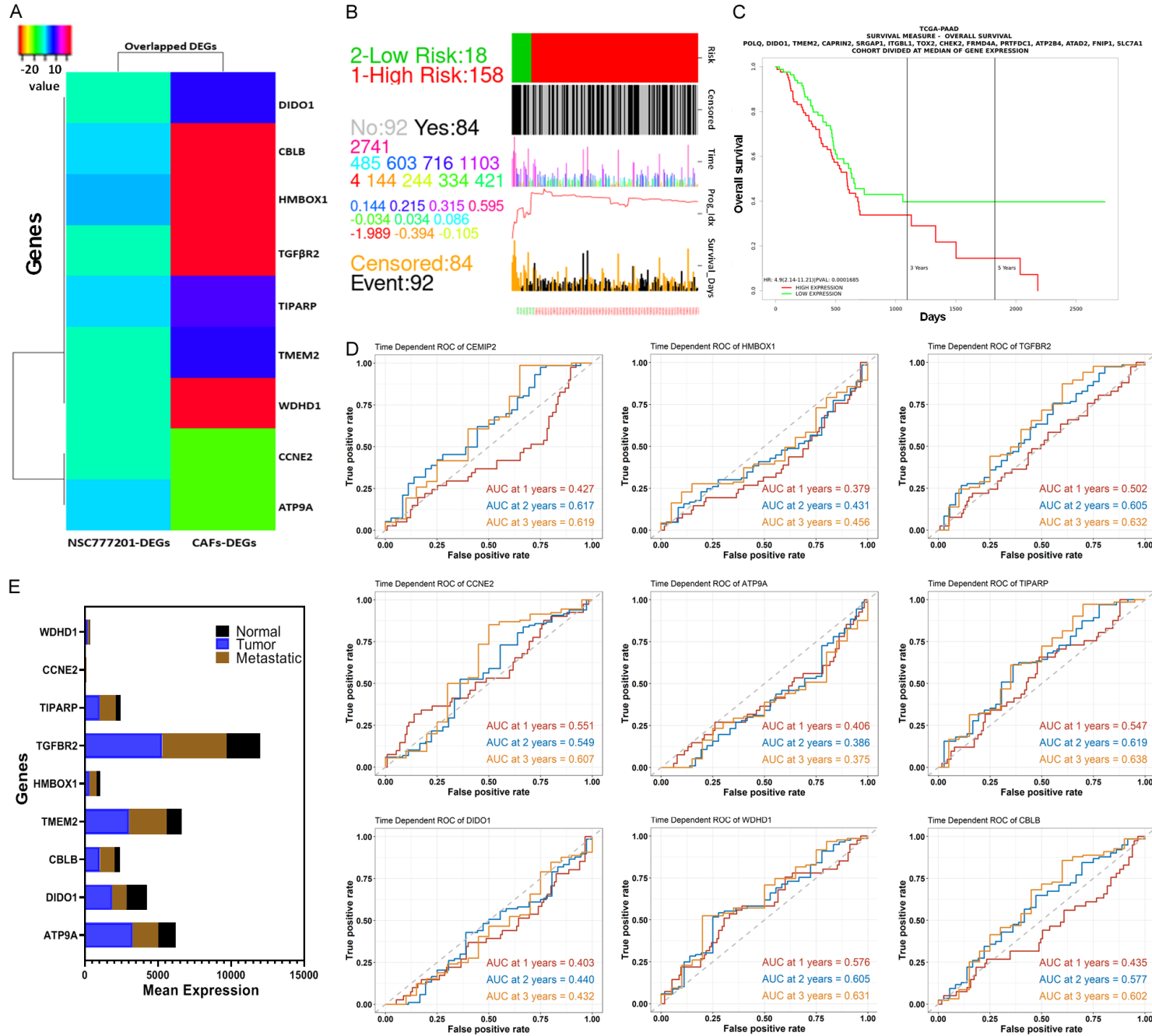TMEM2 in pancreatic cancer: biomarker analysis & NSC777201 drug potential

Figure 3. Prognostic value of nine common overlapping differentially expressed genes (DEGs). A. Heat map of nine overlapping DEGs. B. The SurvExpress database (http://bioinformatica.mty.itesm.mx:8080/Biomatec/SurvivaX. jsp; accessed 6 August 2021) was applied to analyze associations of the nine-gene signature with the predictive risk, survival time, and prognosis, with gene expression levels in high- and low-risk groups. C. Kaplan-Meier survival curve showing that patients in the high-risk group had a poor prognosis, i.e., those with higher expression levels of the combined nine DEGs demonstrated lower survival times (hazard ratio =4.9 (95% confidence interval =2.14~11.21); P=0.0001685). An online protocol was used (http://www.progtools.net/gene/results.php; accessed 6 August 2021) to analyze the association of the nine DEG signatures with the predicted risk. D. An ROC analysis was performed to compare the sensitivity and specificity of the survival prediction, and $P<0.05$ was considered statistically significant. R-package, timeROC, and pROC were used to generate the plot. E. Expressions of the nine DEGs in pancreatic adenocarcinoma (PAAD), metastasis, tumor, and normal samples. TNM plot (https://tnmplot.com/; accessed 6 August 2021) was used to download the expression data. Data were plotted using GraphPad Prism 9. Prog. Idx., Prognosis Index. *$P<0.05$.

description of protein expressions in human cells and tissues, providing a basis for tissue-based diagnostic and translational research. From this analysis, we observed that TMEM2 at the protein level was highly or moderately expressed in liver cancer (35% high and 65% moderate), PC (25% high and 75% moderate), and thyroid cancer (25% high and 75% moderate) patients compared to other different cancers (**Figure 5A**). We also observed medium expression levels of the TMEM2 protein in normal pancreatic tissues (**Figure 5B**); from further analysis, we observed that TMEM2 was mostly expressed in vesicles and plasma membranes, suggesting its enzymatic role as a predominant mediator of contact-dependent hyaluronan (HA) and focal adhesion (FA). HA degradation and remodelling of the microenvironment favour tumor growth and invasion [52]. IHC samples from the HPA database corresponded to our previous observations, i.e., the protein level of TMEM2 was upregulated in PC tissue samples compared to normal tissues (**Figure 5C**), bar plot (also shown below) to demonstrate the number of patients showing negative, weak, moderate or strong expression, we observed cancer samples are showing strong (n=3) and moderate (n=8) expression of TMEM2 as compared to normal (moderate, n=3). Confirming the cancer showing higher expression of TMEM2 at the protein level.

TMEM2 correlated with CAF expression in PAAD

In the second phase of this study, a thorough analysis was conducted to investigate the association of TMEM2 expression and the impact of CAF-associated genes in PAAD. A shortlist of important known CAF-associated and -related markers, viz., ACTA2, FAP, FN1, PDGFA, PDGFB, S100A4, SMAD2, TGFB1, and VIM, were analyzed, and their expression patterns at both the mRNA and protein levels were compared and correlated with TMEM2 expression in PAAD samples. As shown in **Figure 6A**, a heatmap (left panel), and combined correlation plot (right panel) denoted the strong correlations of TMEM2 with CAF markers, especially FAP (r= 0.482; P=9.83E-12), FN1 (r=420; P=1.20E-08), and ACTA2 (r=0.420; P=2.60E-07). Furthermore, in **Figure 6B**, CAF-associated markers were observed to be strongly co-expressed in the high-risk PAAD patient group compared to the low-risk group, especially expressions of FAP, FN1, S100A4, and SMAD2. CAF genes were significantly overexpressed in the high-risk group of patients compared to the low-risk group. In **Figure 6C**, interestingly, the IHC analytical data of HPA demonstrated that co-expression correlations at the protein level also followed the trend, that is, at the protein level expression, FAP was strongly associated with TMEM2 expression in human PC compared to other CAF markers. The co-expression correlations of these markers were also evaluated in normal pancreatic samples, and results demonstrated that all the markers were not detected or detected at very low levels in normal tissues, except for SMAD2, PDGFA, PDGFB, and VIM. These results denoted that in a cancerous condition, the markers of S100A4, FN1, FAP, ACTA2, and TGFβ1, which were not detected in normal tissues, may play oncogenic roles, especially FAP expression might modulate the expression of TMEM2 to pave a favourable path for tumor growth and metastasis (**Figure 6C**; lower panel).

IPA and downstream biological function analysis of DEGs associated with the response of Panc1 cells to NSC777201

Next, we performed an IPA of DEGs in Panc1 cells in response to NSC777201. The IPA core

A

TMEM2 differential plot

B

The median expression of Tumor and normal samples in body map

Pancreas : 5.65

Pancreas : 3.39

Tumor

Normal

Log₂(TPM + 1) Scale

C

Expression of TMEM2 in PAAD based on individual cancer stages

*

*p-value <0.05

D

P = 3.77e-06

TNMplot							
	Min	Q1	Med	Q3	Max	Upper whisker	N
Normal	106	316	542	757	3253	1310	108
Tumor	41	520.5	783	1174.5	2769	2091	248
Metastatic	22	366	821	1189	1780	1780	17

E

CEMIP2

HR = 1.64 (1.06 - 2.52)
logrank P = 0.023

Expression
— low
— high

Number at risk				
low	130	46	13	7	1
high	47	12	4	1	0

F

2-Low Risk:18
1-High Risk:158

No:92 Yes:84

2741
485 603 716 1103
4 144 244 334 421

0.144 0.215 0.315 0.595
-0.034 0.034 0.086
-1.989 -0.394 -0.105

Censored:84
Event:92

Risk

Censored

Time

Prog. Idx

Survival Days

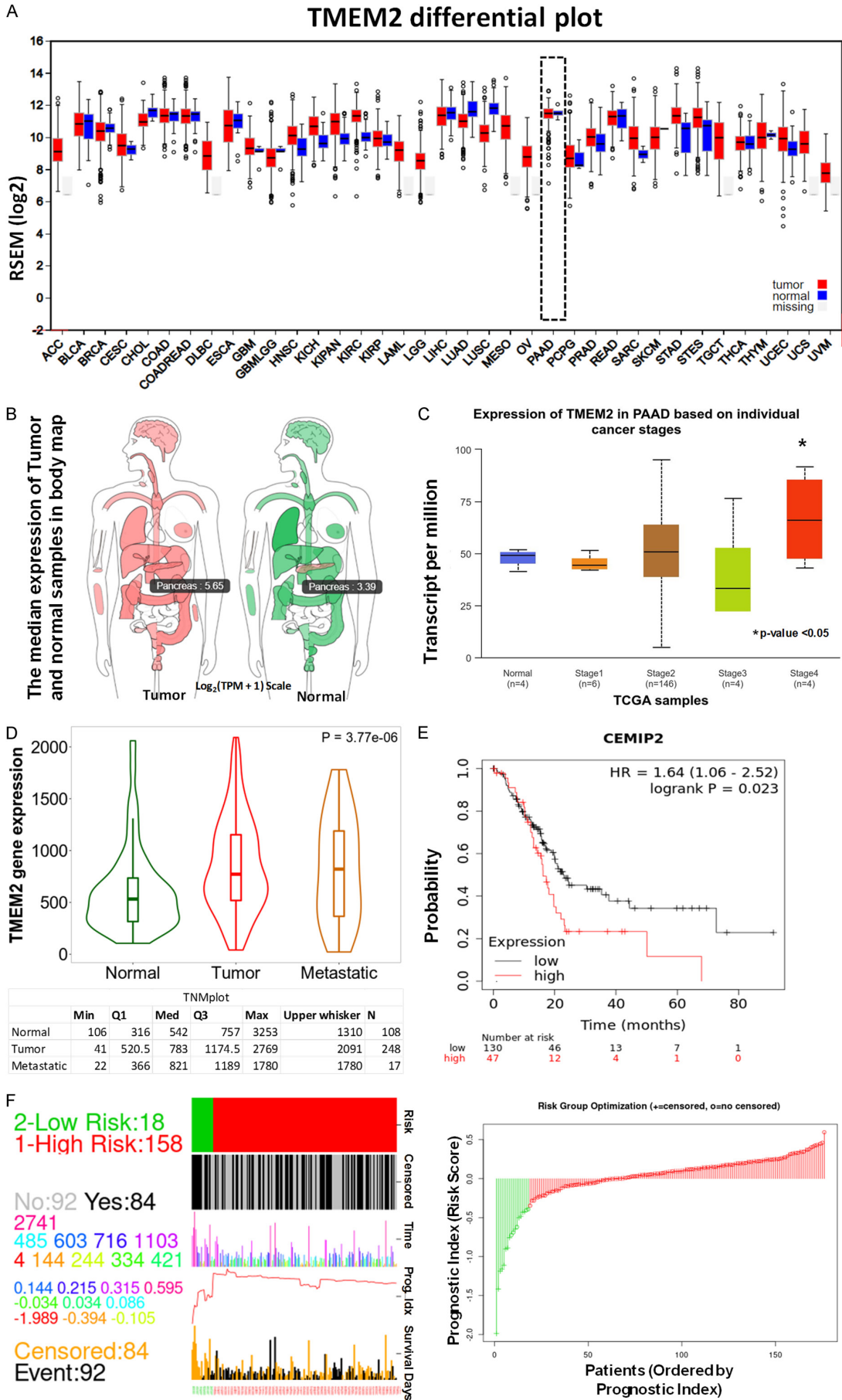Risk Group Optimization (+=censored, o=no censored)

Figure 4. Expression distribution of transmembrane protein 2 (TMEM2 or CEMIP2) in pancreatic adenocarcinoma (PAAD) patients. A. Expression distribution of TMEM2 in different tumors in TCGA database (https://gdac.broadinstitute.org/; accessed 7 August 2021). B. Median expression levels of TMEM2 in tumor and normal human pancreatic tissues in a body map (http://gepia.cancer-pku.cn/; accessed 7 August 2021). C. TMEM2 expression levels in PAAD patients based on individual cancer stages (http://ualcan.path.uab.edu/cgi-bin/ualcan-res.pl; accessed 9 August 2021). D. TMEM2 expression levels in metastasis, tumor, and normal samples (https://tnmplot.com/; accessed 9 August 2021). E, F. KM plot database (https://kmplot.com, accessed 19 April 2024) and the SurvExpress database were used for Kaplan-Meier survival analysis and to predict TMEM2 with the predictive risk, survival time, and prognosis using gene expression levels in high- and low-risk groups (http://bioinformatica.mty.itesm.mx:8080/Biomatec/SurvivaX.jsp; accessed 9 August 2021).

analysis allowed us to interpret the dataset in the context of biological entities such as canonical pathways, upstream regulators, causal network master regulators, diseases, and biological functions (all of which passed the selection criteria of $P<0.05$ and z-score >2), whereas an orange node represents predicted activation (z-score >2) and a blue node represents predicated inhibition (z-score <-2) [48]. As described in the overall summary of the IPA, we observed activation of significant pathways, such as replicative senescence of fibroblast cell lines, replicative senescence of cells, and cytostasis (inhibition of cell growth and multiplication) as denoted by a higher-intensity orange color. Significant inhibition of cell movement of tumor cell lines, cell proliferation of carcinoma cell lines, and colony formation of tumor cells are denoted in blue with a higher intensity (**Figure 7A**) after NSC777201 treatment of Panc1 cells. Furthermore, based on our analysis, we identified several disease-associated or biological function-associated pathways (**Figure 7B**). Importantly, the cell-to-cell signaling interaction ($P<0.05$), cellular movement ($P<0.05$), cell growth and proliferation ($P<0.05$), and hematological system development ($P<0.05$) were the most suppressed (blue; z-score ≤2) pathways. Interestingly, a few pathways were significantly activated (orange; z-score ≥2), such as replicative senescence of fibroblast cell lines ($P<0.05$), replicative senescence of cells ($P<0.05$), inhibition of cell movement, and cellular growth and division ($P<0.05$) (lower panel, **Figure 7B**). These results suggest that NSC777201 treatment can inhibit cancer cell proliferation and induce the senescence of fibroblast cells in a predictive manner.

Molecular docking elucidates the binding mode of NSC777201 with TMEM2

As the TMEM2 protein is overexpressed in PAAD, we wanted to elucidate the mechanism of TMEM2 inhibition. Using computer-based drug target prediction software SwissTargetPrediction (http://www.swisstargetprediction.ch/) for NSC777201 as a query molecule, we identified the top predicted targetable proteins, among which were enzymes (26.7%), proteases (26.7%), kinases (13.3%), family A G protein-coupled receptors (13.3%), electrochemical transporters (13.3%), and hydrolases (6.7%) as shown in Figure S5. We, therefore, performed a computational docking analysis of the NSC777201 compound docked in the active site of TMEM2. For docking the TMEM2 target protein (Q9UHN6; left side, **Figure 8A**), its structure was downloaded from the uniport website, and the chemical 3D structure of the ligand (NSC777201; right side, **Figure 8A**) was prepared. Protein-ligand docking was performed with the entire protein structure using the automated CB-Dock server [49] and visualized by the Discovery studio visualizer vers. 21.1.0.20298, (BIOVIA, San Diego, CA, USA) [51]. Blind docking was performed to detect suitable binding sites for a ligand onto the protein by adjusting the cavity centre and docking box size. The result of docking demonstrated that NSC777201 stably docked in the binding cavity of TMEM2 (**Figure 8B**) and docking energies for each docking mode and docking box size were calculated (below, **Figure 8B**). The legend-receptor complex was stabilized through various hydrogen bonds and alkyl, van der Waal, and carbon-hydrogen bond interactions. Studies showed that NSC777201 interacted with TMEM2 with an utmost binding affinity score of -6.8 kcal/mol, demonstrating a high drug interaction, whereas, as shown in **Figure 8C**, NSC777201 occupied the active site of the target protein. Furthermore, the docked conformation of NSC777201 with its interacting residues is shown in **Figure 8D**. NSC777201 interacted with THR(A):246, ASN(A):246, and THR(A):1339 at respective distances of 2.95, 4.54, and 3.77 Å, via conventional hydrogen bonds. Although alkyl and

A Human Protein Atlas: TMEM2 Expression in Cancers
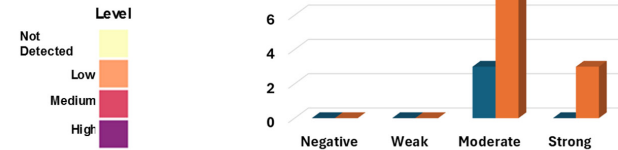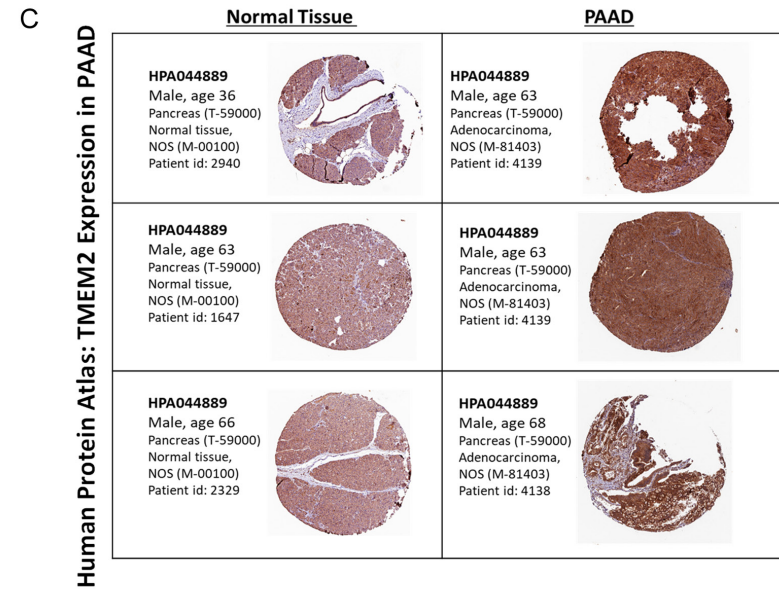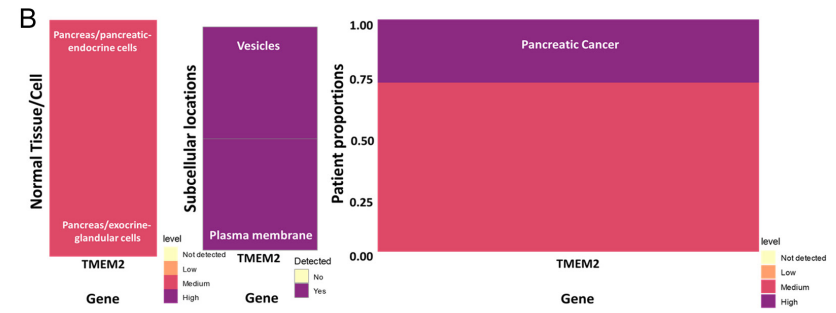
B

C Human Protein Atlas: TMEM2 Expression in PAAD

Figure 5. Detection of TMEM2 and cancer-associated fibroblast (CAF) marker expressions by IHC in human cancer tissues. A. Histogram of TMEM2 and CAF marker expressions in 20 different human cancers from the Protein Atlas (www.proteinatlas.org/, accessed 10 September 2021). IHC staining was evaluated as high/medium/low staining or not detected, and the histogram and tissue/cell subcellular expression intensities were visualized using the HPA-analyze R package. TMEM2 was highly expressed in pancreatic cancer compared to other cancer types. B. Expression levels of TMEM2 in tissues and cells, subcellular location, and expression proportions in pancreatic cancer. C. Representative IHC staining of TMEM2 in pancreatic adenocarcinoma (PAAD) and normal samples present in the HPA database, Bar charts depict the number of cases with different IHC staining intensities.
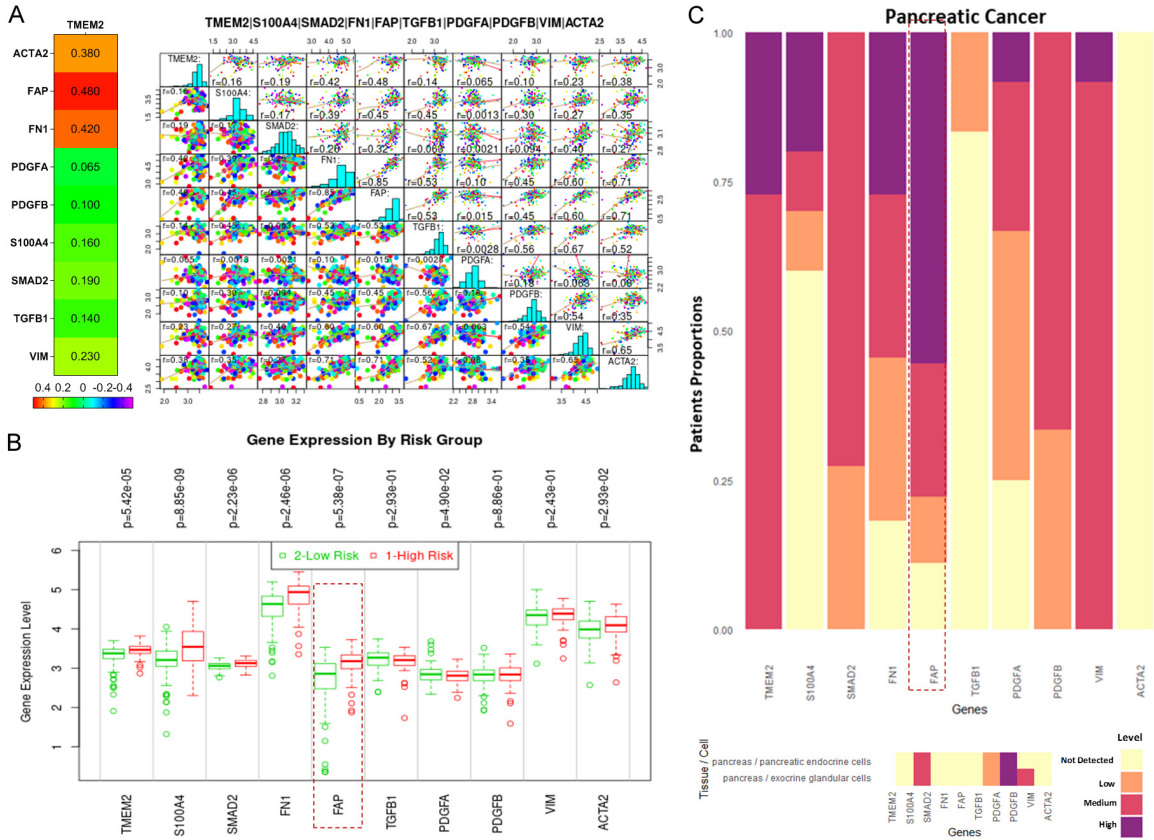
Figure 6. Correlation and risk associated with expressions of TMEM2 and CAF markers and associated genes in TCGA-pancreatic adenocarcinoma (PAAD) datasets. A. Correlation plot of TMEM2 and CAF marker expressions in PAAD patients, and a heatmap showing correlation coefficients. B. A box plot confirming higher expressions of TMEM2 and CAF-related genes in the high-risk group than in the low-risk group using a *t*-test. C. Histogram of TMEM2 and CAF marker expressions in PAAD from the HPA; the histogram and tissue/cell subcellular expression intensities were visualized using the HPA analyze R package.

pi-alkyl interactions occurred with LYS(A):278 and LEU(A):280, at respective distances of 4.80 and 5.48 Å with Cl atoms of NSC777201, LYS(A):278 formed another interaction via pi-alkyl bonds at a distance of 6.38 Å. Furthermore, pi-pi T-shaped interactions emerged at respective distances of 6.82 and 7.37 Å with PHE(A):254 and PHE(A):1338. Meanwhile, PHE(A):254 established pi-sulfur bonds at a distance of 6.84 Å of NSC777201, whereas ASP(A):273, LYS(A):1318, THR(A)276, VAL9A):386, LEU(A):1337, ASP(A):387, ARG(A):245, and GLU(A):474 interacted with NSC-777201 through van der Waals forces, and carbon-hydrogen bond interactions at a distance of 3.64 Å with the PRO(A):253 residues. Furthermore, there was one unfavourable LYS(A):1336 interaction with NSC777201 at a distance of 7.24 Å. Collectively, the results of our computational study further reinforced that NSC777201 is a novel drug that is a key inhibitor of TMEM2 and can improve PC therapy.
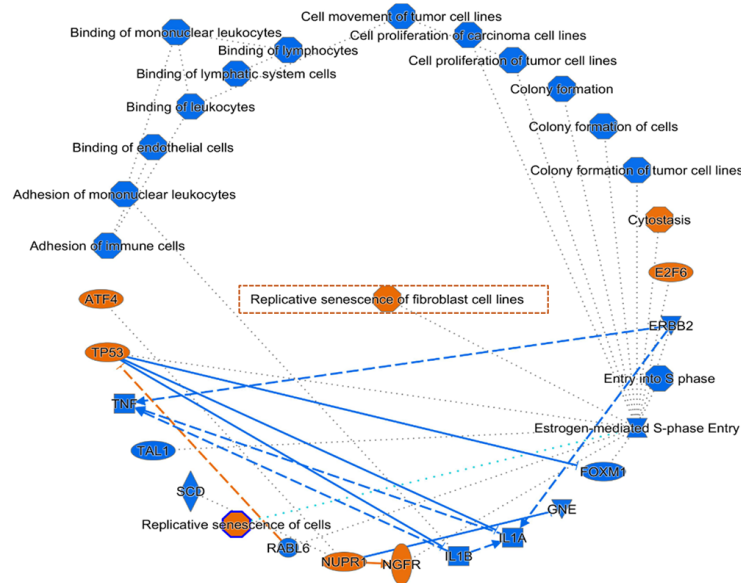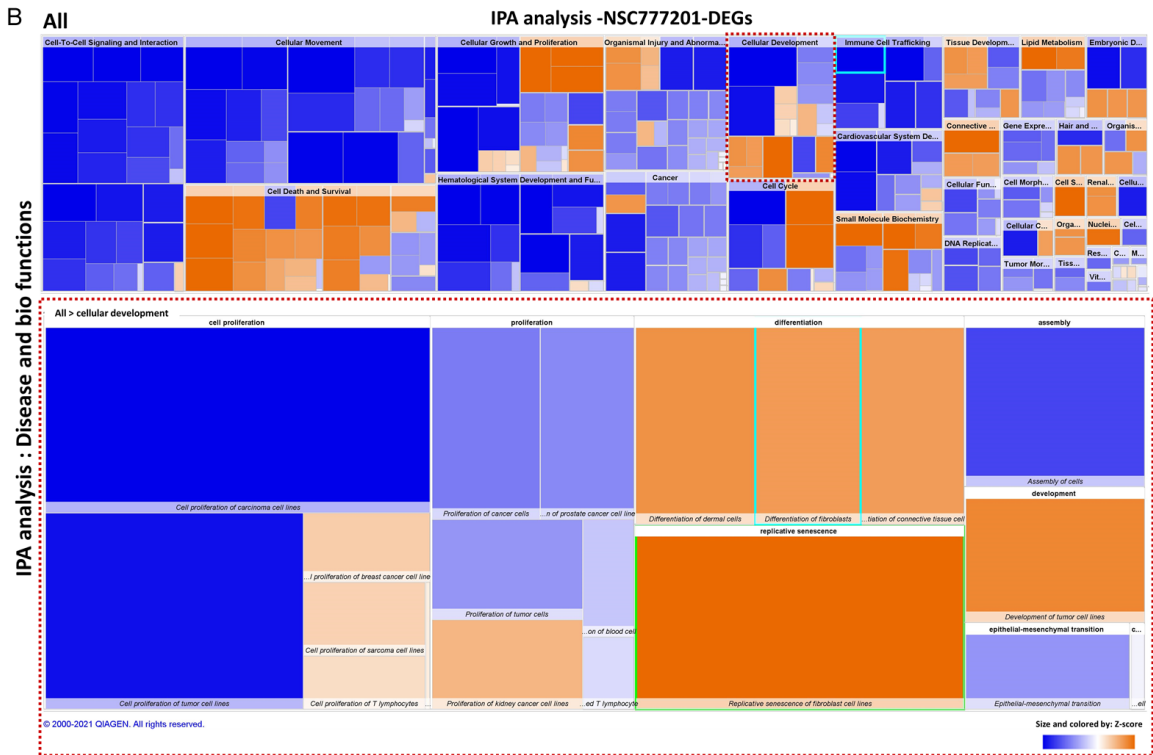
Figure 7. Ingenuity Pathway Analysis (IPA) summary and downstream effector analysis of NSC777201-associated DEGs. A. Overall summary representing the regulatory effect of NSC777201 treatment on Panc1 pancreatic cancer cells. B. Visualization of a hierarchical heat map (TreeMap) depicting affected functional categories based on the DEGs where the major rectangular boxes represent the category of disease and functions. Each individual-coloured box is associated with a particular biological function or disease, and the colour indicates its predicted activation state of induced (orange) or reduced (blue). The size of the rectangles is correlated with the overlap significance. Negative Z-scores indicate the downregulation of a biological function, while positive Z-scores indicate the upregulation of a function. Absolute Z-score values of >2.0 were used to make biological predictions. Significant inhibition of cancer cell proliferation and activated replicative senescence was observed after NSC777201 treatment.
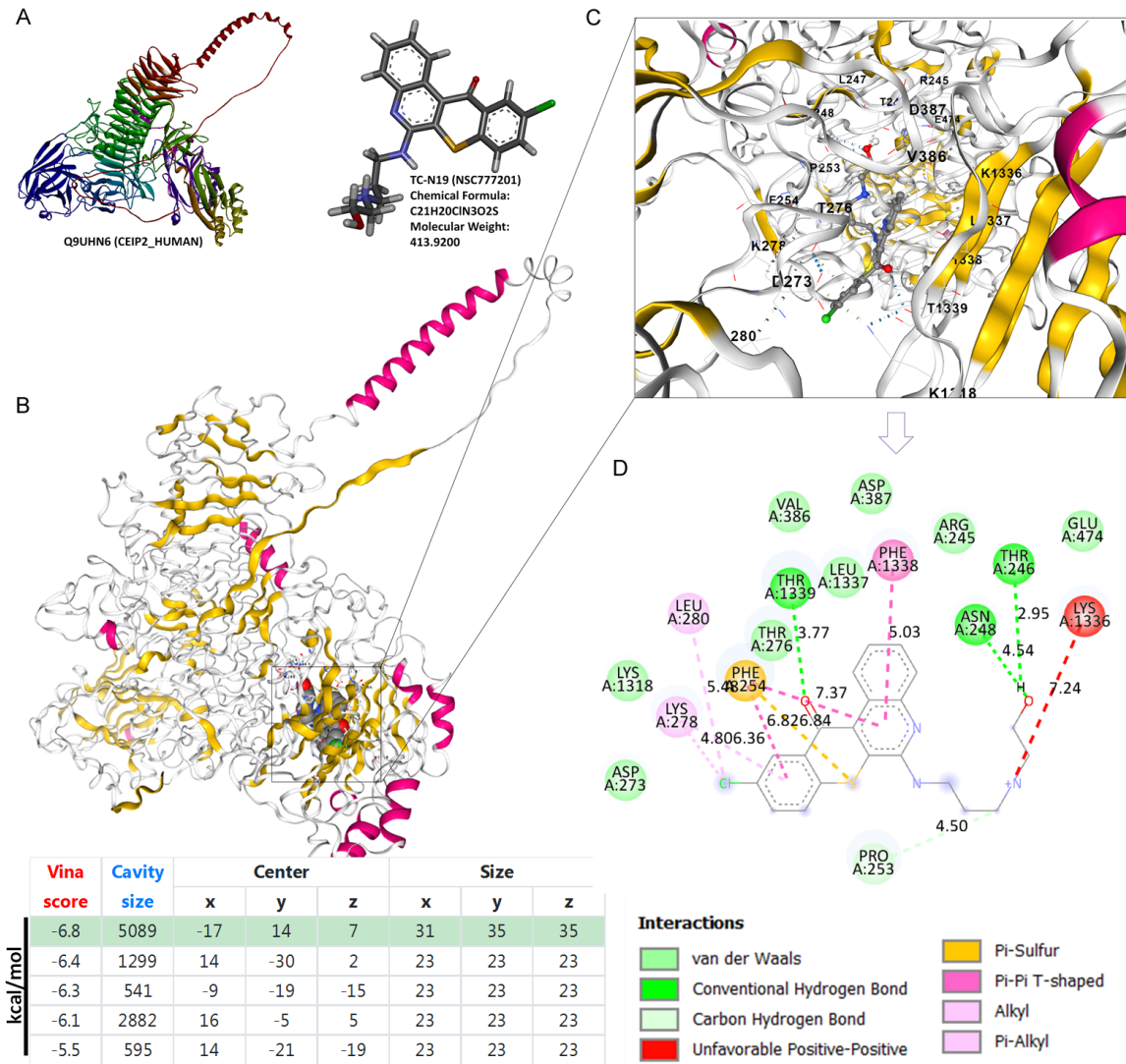
Figure 8. Visualization of molecular docking analysis of binding of NSC777201 with TMEM2. A. The structure of TMEM2 (CEMIP2) [Uniprot ID: Q9UHN6], and the chemical structure of NSC777201. B. The coupling of NSC777201 with TMEM2 active canter residues, and the binding affinity, cavity size and coordinates. C. The enlarged 3D image shows the binding of NSC777201 with different bonds with acceptor amino acid residues of TMEM2 to stabilize the binding complex in the cavity. D. The 2D plot shows the interaction of the binding pocket residues with the NSC777201.

In-vitro validation of the impact of siRNA and pharmacological (NSC777201) inhibition effect on TMEM2

In-vitro study illustrated in **Figure 9**, the effects of TMEM2 inhibition on various pivotal cellular processes associated with cancer progression were examined. In **Figure 9A** and **9B**, expression both at protein and mRNA levels analyzed by western blot and real-time RT-PCR, we observed a noticeable dysregulation in the expression of TMEM2 at both protein and mRNA levels post-inhibition, lending confiden-

ce to the efficacy and specificity of inhibitory approach. In the cell viability assay depicted in panel **Figure 9C**, TMEM2 inhibition demonstrated a significant reduction in cellular viability, emphasizing TMEM2's key role in orchestrating cellular survival dynamics. Further, as explained in **Figure 9D**, **9E**, the inhibition of TMEM2 indicated an evident decline in the tumor sphere formation and cellular migratory activities, highlighting TMEM2's essential role in driving tumor aggressiveness (stem cell behaviour) and invasiveness. The **Figure 9F** elucidates that the strategic inhibition of
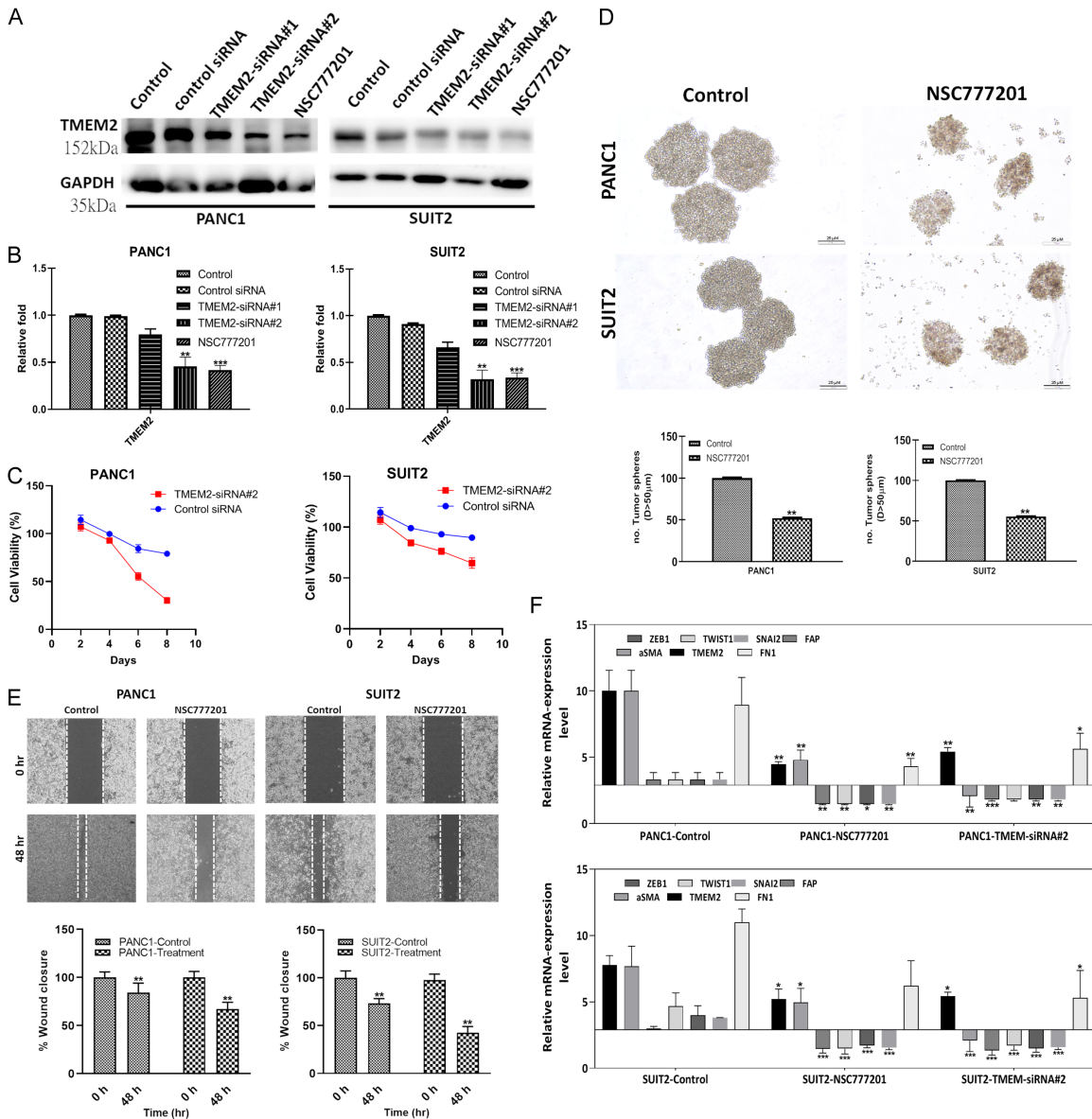
Figure 9. *In-vitro* validation of the impact of TMEM2 inhibition. A, B. Western-blot and qRT-PCR analysis showing the siRNA-mediated inhibition of TMEM2 in Panc1 and Suit2 cells. C. Impact TMEM2 inhibition on the viability of both the cells measured using SRB cell viability assay. D, E. Self-renewal and migratory ability of both the cells were evaluated by tumor sphere and migration assay after TMEM2 knockdown. F. qRT-PCR analysis demonstrated inhibition of TMEM2 in Panc1 and Suit2 cells, respectively inhibiting key CAFs marker expression, and importantly FAP expression. ***P<0.001; **P<0.01; *P<0.05.

TMEM2 led to a consequential decline in the expression of pivotal CAF markers across the Panc1 and Suit2 cells. Lastly, to validate NSC777201 targeting TMEM2, the rescue experiment was performed as shown in Figure S6A, S6B, sh-TMEM2 transfection treated induced the suppression of sphere-forming abilities of Panc1 tumor sphere, while those can be significantly reversed when treated together with NSC777201-TMEM2-OE (over

expression) when compared to control. Interestingly, at the protein level (Figure S6C), TMEM2 expression was rescued by TMEM2-OE, as compared to control and sh-TMEM2. The results showed the inhibitory effect of the sh-TMEM2 treated Panc1 tumor sphere ability, and the rescue effect of TMEM2-OE, abrogating the NSC777201 effect. This observation underscores TMEM2's influential modulation of the CAF phenotype, thereby revealing new

insights into our understanding of the intricate interplay between TMEM2 and the cancer microenvironment.

In-vivo preclinical validation

After establishing NSC777201's anti-PAAD effect functions *in-vitro*, the *in-vivo* preclinical effects of NSC777201 targeting xenograft mouse Panc1 tumor model. The tumor size over time clearly showed that NSC777201 treatment alone or sh-TMEM2 resulted in significantly delayed tumorigenesis, while the vehicle control groups showed induced tumor growth. Notably, NSC777201 and sh-TMEM2 groups showed the most significant delays in tumorigenesis (**Figure 10A**, **10B**). Using a Kaplan-Meier survival curve, we verified that NSC777201, sh-TMEM2 conferred a significant survival advantage in mice, compared to the vehicle-control groups (**Figure 10C**). The qPCR analysis of plasma levels of TMEM2 showed the reduced level in NSC777201 and sh-TMEM2 treated pooled blood samples, in comparison to vehicle control (**Figure 10D**). Comparative western blots and qRT-PCR analysis of tumor samples collected in all groups demonstrated reduced TMEM2 and FAP expression (**Figure 10E**, **10F**). Taken together, these data suggest that the downregulation of TMEM2 expression in PAAD carcinoma cells effectively inhibits the formation and growth of PAAD cancer *in-vivo*.

Discussion

Recently, the application of novel chemotherapeutic drugs and surgical interventions has partially improved PAAD treatment. However, most patients with PAAD are diagnosed at an advanced stage with poor survival and therapeutic resistance resulting in higher PAAD patient mortality [53, 54]. As PAAD is one of the most serious solid tumors, the increased stromal content is one of the PAAD hallmarks features [55]. In the TME, the most dominant components in the tumor stroma are CAFs, which are spindle-shaped cells that build up and remodel the ECM [56]. However, the "CAF population" remains poorly understood in terms of its origin, subtypes, and biology due to higher heterogeneity and lack of specific markers in PAAD [57, 58]. Another important member of the ECM is hyaluronan (HA); its abnormal metabolism and accumulation particularly the small HA oligosaccharide (LMM-HA), as an independent prognostic factor for poor survival in

PC [59], are key hallmarks of cancer [60, 61]. HA is known to be metabolized by HA-enzyme-hyaluronidase enzymes such as HYAL1, -2, and -3, and KIAA1199 is also known as CEMIP [62-64]. Activation of these enzymes reportedly showed aberrant expressions in many cancers [29]. In particular, HYAL1 and KIAA1199 are significantly overexpressed in PC, and inhibition of these enzymes results in the reduced migratory ability of PC cells [30, 31]. Nevertheless, how CAFs modulate their expressions and are associated with HA-enzyme activation is still not studied well.

Therefore, in this present exploration, we conducted a comprehensive *in silico* approach intended to identify a key gene, as well as the potential of the novel NSC777201's effect on inhibiting PAAD. We screened DEGs from the GEO database (GSE172096), i.e., from CAF compared to NF samples (**Figure 1**) and performed functional enrichment and pathway analyses of these identified DEGs (Figure S2). Furthermore, the function and pathway enrichment analyses found that the most significant pathway was "pathways in cancer", whereas those of functional categories were "DNA replication" and "DNA integrity checkpoint". In addition, to investigate the effect of the novel NSC777201's effect on PC Panc1 cells, microarray gene expression profiling was performed. NSC777201 treatment modulated expressions of many key DEGs, and after overlapping these NSC777201-associated DEGs with CAF-associated DEGs, we observed nine genes in common (**Figure 2**). These nine overlapping NSC777201-associated DEGs were further screened by a Cox multiple regression analysis of PAAD RNA-sequencing data from TCGA. The KM survival analysis indicated that patients at high risk corresponded with shorter OS times than patients with low-risk scores (*P*<0.0001). The AUC of this model was an average of 0.6 at 12 months OS, indicating that the predictive value of the nine-gene signature could be utilized for survival predictions. Compared to other specific medical parameters (including age, sex, tumor stage, and histological type), risk scores were better predictors of patient survival, indicating that the nine-gene signature may be of value in further research (**Figure 3**).

Interestingly, among the nine overlapping DEGs, TMEM2 or CEMIP2 expression was negatively correlated with OS times of PAAD patients.
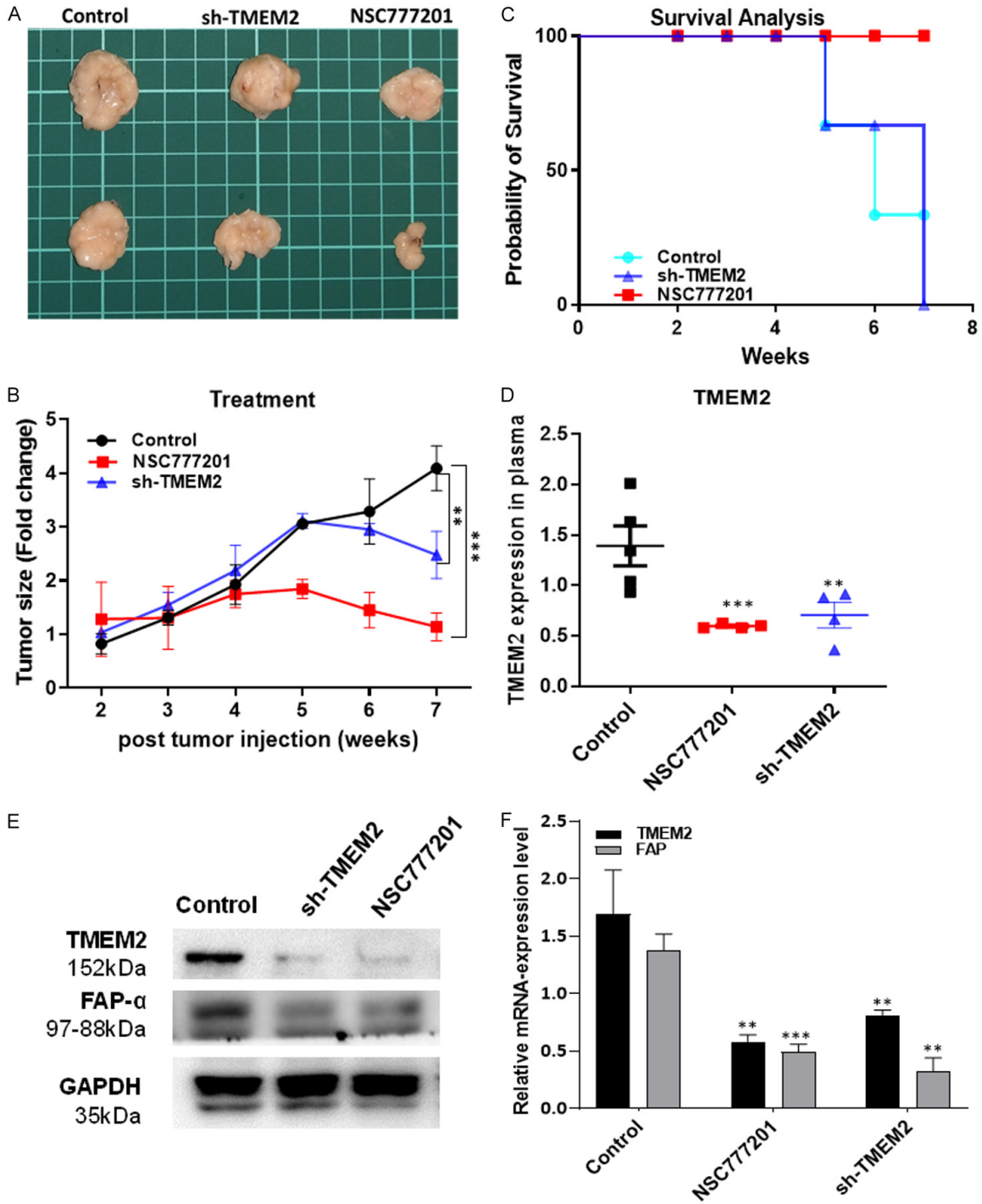
Figure 10. Efficacy evaluation of NSC777201 using a Panc1 cells xenograft mouse model. (A) The insert shows representative photographs of tumor samples from each group, (B) tumor size over a time curve. The tumor growth delay was most significant in the NSC7777201 treatment group, followed by the sh-TMEM2-only group, while vehicle control groups showed a significant difference in tumor size. (C) Kaplan-Meier survival curve, mice receiving NSC777201, or sh-TMEM2 only showed the highest survival ratios, while control mice showed the lowest survival ratios. (D) qPCR analyses of plasma levels of TMEM2. Pooled blood samples from all four groups of mice were analyzed for TMEM2 plasma levels. The NSC777201, or sh-TMEM2 only showed the lowest level followed by control. (E) Tumor sample western blot analysis. Expressions of TMEM2 and FAP were lower in samples from NSC777201, or sh-TMEM2 treated tumors. (F) qPCR analyses of tumor samples from all three groups of mice were analyzed The NSC777201, or sh-TMEM2 only showed the lowest level of TMEM2 and FAP expression. *$***P<0.001$; $**P<0.01$; $*P<0.05$.

TMEM2 is a cell-surface hyaluronidase and a potent modulator of matrix-associated HA, and TMEM2 activity is necessary for cells to achieve robust cell adhesion and migration on HA-containing substrates [52]. TMEM2 has been implicated in the aggressive behavior of many solid cancers, with the studies linking it to poor outcomes in many cancers [65, 66]. Importantly, Lee et al. utilized the Gene Expression-based outcome for breast cancer online tool to find that TMEM2 expression correlated with worse prognosis in grade 3 breast tumors, especially within the luminal B and HER2-positive categories via SOX4 regulation [65]. Study reported by L. Gan et al. demonstrated the inhibition of TMEM2 results in the reduced invasion and migration of breast cancer through the modulation of JAK/STAT3 signaling [67]. Similarly, in gliomas, increased TMEM2 expression not only escalates with tumor grade but also serves as a distinct prognostic marker for refining molecular subtypes and predicting outcomes more accurately [66]. Despite these associations, the precise mechanisms through which TMEM2 influences cancer progression warrant further investigation.

Our study contributes to this body of knowledge by demonstrating a significant upregulation of TMEM2 in PAAD tumors compared to normal tissue, a finding consistent across a diverse array of 37 cancer types. Notably, TMEM2 levels were markedly higher in advanced stages of PAAD, correlating with decreased patient survival (**Figures 4, 5**). These observations position TMEM2 as a critical biomarker for diagnosis, and prognosis, and as a potential target for therapeutic intervention in PAAD, signifying its importance in future research endeavours. Furthermore, our examination extends into the intricate environment of PC, which is characterized by a mix of transformed cancer cells at varying stages of the epithelial-mesenchymal transition (EMT) and an assortment of non-transformed stromal cells. This stromal compartment, comprising cancer-associated fibroblasts (CAFs), macrophages, and a variety of immune, endothelial, and epithelial cells, plays a significant role in the tumor microenvironment (TME) [68, 69].

CAFs are one of the prominent and active components of the pancreatic TME, and classical CAF markers are characterized by induced expression of alpha-smooth muscle actin (α-SMA), FAP, fibroblast-specific protein 1 (FSP1) or S100A4, platelet-derived growth factor receptor (PDGFR)-α/β, and vimentin (VIM), all recognized as contributors to carcinogenesis [57, 70]. The activation of canonical SMAD2 signaling, culminating in the elevation of TGFβ1 and FN1, further denotes the abundance of CAFs, highlighting their significance in the PC landscape [71, 72]. This detailed understanding of the PC microenvironment, along with the pivotal role of TMEM2, underlines the complexity of cancer progression and the potential avenues for therapeutic intervention. Our results demonstrated that TMEM2 expression at both the mRNA and protein levels was strongly correlated with expressions of FAP (r=0.480), FN1 (r=0.420), and S100A4 (r=0.380) in PAAD, and higher expressions of FAP (P=5.38 × 10⁻⁷), FN1 (P=2.46 × 10⁻⁶), and S100A4 (P=8.85 × 10⁻⁹) were significantly correlated with the high-risk group in PAAD (**Figure 6**). CAF roles are in forming 'cancerized' fibrotic stroma favourable to tumor initiation, progression, stemness, dissemination, metastasis, and drug resistance via remodelling of the ECM through activation of hyaluronidase [73]. The activation of TMEM2 was suggested to be indirectly or directly associated with the expression of CAFs mainly with classical CAFs associated with the FAP gene, which plays a pivotal role in tumor initiation through the metabolism of HA. Hence, the identification of novel small molecules with the potential to inhibit the HA enzyme and modulation of CAF expression is crucial. Our team previously reported the importance of NSC777201 in inhibiting lung cancer tumorigenesis [38]. However, the effect of NSC777201 on ECM modulation still needs exploration, especially in PAAD tumorigenesis. Herein, we performed an IPA analysis to investigate the effect of NSC777201 on gene expressions and associated pathway modulation in PAAD, and results demonstrated significant activation of replicative senescence of fibroblast cell lines, cell death, apoptosis, (z-score >2), and inhibition of cellular development, cell proliferation, and the EMT (z-score <-2). The *in-silico* study results suggested that NSC777201 is a novel molecule that exhibits potential to target PAAD through modulating the CAF-HA-enzyme axis (**Figure 7**).

Interestingly, to further demonstrate the predictive target of NSC777201, we applied the SwissTargetPrediction online computational tool (http://www.swisstargetprediction.ch/),

Flow of study
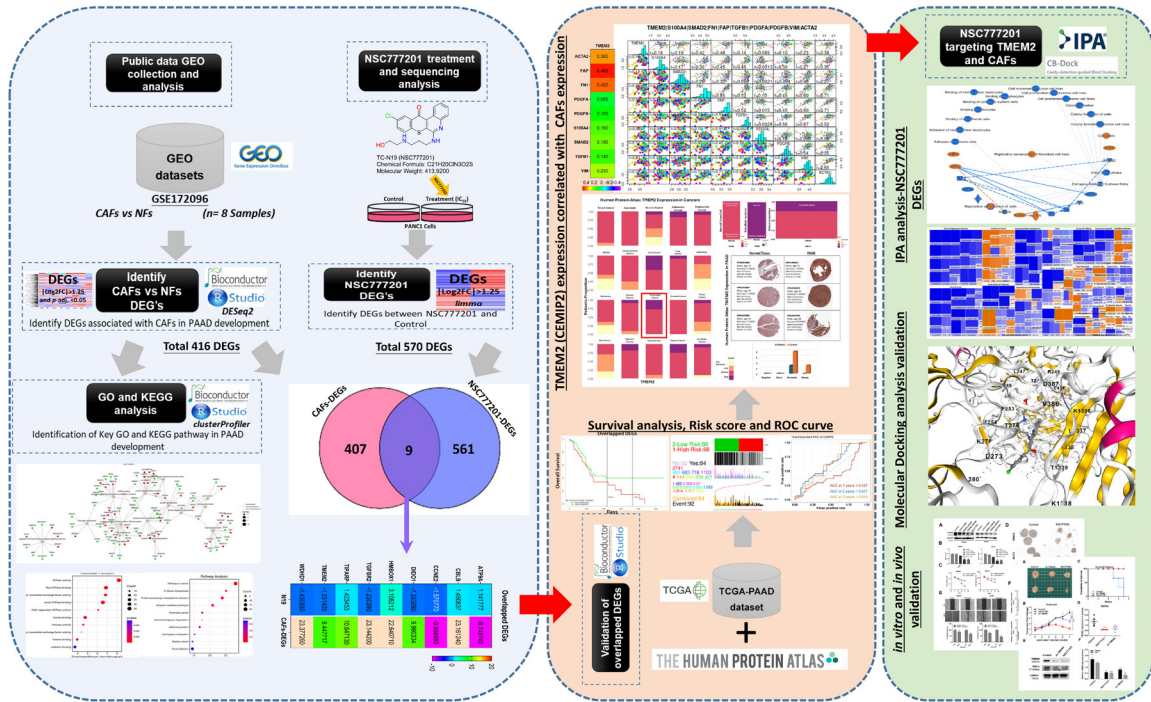
Figure 11. Overall study flow (left to right). Common DEGs identification between public and in-house sequencing data. Key gene (TMEM2) identification and its prognostic values, together with its expression analysis in PAAD from different (both RNA and protein) databases, correlation analysis with CAFs markers, IPA analysis of DEGs identified after the NSC77201 drug treatment in Panc1 cells, to predict key pathways inhibited or activated after treatment. Molecular docking to show predictive binding of drug with TMEM2, *in-vitro* and *in-vivo* validation. The current study was designed to explore the importance of TMEM2 a HA enzyme, in the PAAD TME, together with the role of CAFs, interestingly the newly discovered molecule NSC777201 can also modulate the expression of TMEM2, which results in the alteration of PAAD-TME and its progression.

and the top predicted and significant targetable proteins identified were enzymes (26.7%) and proteases (26.7%). Therefore, an *in silico* molecular docking analysis of NSC777201 was also performed on TMEM2, and results demonstrated in **Figure 8**, that NSC777201 showed a higher binding affinity with TMEM2 with the lowest energy conformation (-6.8 kcal/mol), the ligand-and-receptor complex was stabilized through various hydrogen bonds and alkyl, van der Waal, and carbon-hydrogen bond interactions, indicating that NSC777201 can be used. Our comprehensive studies demonstrate the profound impact of TMEM2 inhibition on cancer progression through *in-vitro* and *in-vivo* analyses (**Figures 9** and **10**). TMEM2 dysregulation at both protein and mRNA levels confirmed the efficacy of our inhibitory strategy, with subsequent assays indicating a crucial role for TMEM2 in maintaining cellular survival

and promoting tumor aggressiveness (**Figure 9A-E**). *In-vivo*, treatments with NSC777201 and sh-TMEM2 in a xenograft mouse model substantially delayed tumorigenesis and enhanced survival, with reduced TMEM2 and FAP expression corroborating the treatment's effectiveness. Rescue experiments further validated these effects, showing a reversal of TMEM2 suppression through combined NSC777201 and TMEM2 overexpression treatments, which moderated NSC777201's effects (Figure S6). These results highlight TMEM2's significant influence on the cancer microenvironment and its potential as a target for therapeutic interventions, offering new insights into cancer biology and treatment strategies.

Conclusion

In conclusion, our findings, as illustrated in **Figure 11** (overall study design), highlight the

pivotal role of TMEM2 as a significant prognostic and tumorigenic biomarker in the progression of pancreatic adenocarcinoma (PAAD) through its interaction with cancer-associated fibroblasts (CAFs) and modulation of fibroblast activation protein (FAP). These interactions underscore TMEM2's potential as a novel therapeutic target, which could lead to more effective treatments for PAAD. Additionally, NSC777201 emerges as a promising novel small molecule targeting the HA-enzyme, exhibiting substantial anti-PAAD effects. Given its demonstrated efficacy, NSC777201 can serve as an important small molecule drug worthy of therapeutic implications and warrants further investigation to be therapeutically used against PAAD patients.

Disclosure of conflict of interest

None.

Address correspondence to: Alexander TH Wu and Hsu-Shan Huang, Graduate Institute of Medical Sciences, National Defense Medical Center, Taipei 114, Taiwan. Tel: +886-2-6620-2589 Ext. 2-10604; E-mail: chaw1211@tmu.edu.tw (ATHW); Tel: +886-2-6638-2736 Ext. 1377; E-mail: huanghs99@tmu.edu.tw (HSH)

References

[1] Rahib L, Smith BD, Aizenberg R, Rosenzweig AB, Fleshman JM and Matrisian LM. Projecting cancer incidence and deaths to 2030: the unexpected burden of thyroid, liver, and pancreas cancers in the United States. Cancer Res 2014; 74: 2913-2921.

[2] Ferlay J, Partensky C and Bray F. More deaths from pancreatic cancer than breast cancer in the EU by 2017. Acta Oncol 2016; 55: 1158-1160.

[3] Higuera O, Ghanem I, Nasimi R, Prieto I, Koren L and Feliu J. Management of pancreatic cancer in the elderly. World J Gastroenterol 2016; 22: 764-775.

[4] Baek B and Lee H. Prediction of survival and recurrence in patients with pancreatic cancer by integrating multi-omics data. Sci Rep 2020; 10: 18951.

[5] Noone A, Howlader N, Krapcho Ma, Miller D, Brest A, Yu M, Ruhl J, Tatalovich Z, Mariotto A and Lewis DJB. SEER cancer statistics review, 1975-2015. National Cancer Institute 2018; 4.

[6] Oettle H, Neuhaus P, Hochhaus A, Hartmann JT, Gellert K, Ridwelski K, Niedergethmann M, Zülke C, Fahlke J, Arning MB, Sinn M, Hinke A and Riess H. Adjuvant chemotherapy with gemcitabine and long-term outcomes among patients with resected pancreatic cancer: the CONKO-001 randomized trial. JAMA 2013; 310: 1473-1481.

[7] Fischer R, Breidert M, Keck T, Makowiec F, Lohrmann C and Harder J. Early recurrence of pancreatic cancer after resection and during adjuvant chemotherapy. Saudi J Gastroenterol 2012; 18: 118-121.

[8] Erkan M, Hausmann S, Michalski CW, Fingerle AA, Dobritz M, Kleeff J and Friess H. The role of stroma in pancreatic cancer: diagnostic and therapeutic implications. Nat Rev Gastroenterol Hepatol 2012; 9: 454-467.

[9] Liang C, Shi S, Meng Q, Liang D, Ji S, Zhang B, Qin Y, Xu J, Ni Q and Yu X. Complex roles of the stroma in the intrinsic resistance to gemcitabine in pancreatic cancer: where we are and where we are going. Exp Mol Med 2017; 49: e406.

[10] Hanahan D and Weinberg RA. Hallmarks of cancer: the next generation. Cell 2011; 144: 646-674.

[11] Pickup MW, Mouw JK and Weaver VM. The extracellular matrix modulates the hallmarks of cancer. EMBO Rep 2014; 15: 1243-1253.

[12] Shintani Y, Fujiwara A, Kimura T, Kawamura T, Funaki S, Minami M and Okumura M. IL-6 secreted from cancer-associated fibroblasts mediates chemoresistance in NSCLC by Increasing epithelial-mesenchymal transition signaling. J Thorac Oncol 2016; 11: 1482-1492.

[13] Richards KE, Zeleniak AE, Fishel ML, Wu J, Littlepage LE and Hill R. Cancer-associated fibroblast exosomes regulate survival and proliferation of pancreatic cancer cells. Oncogene 2017; 36: 1770-1778.

[14] Ren B, Cui M, Yang G, Wang H, Feng M, You L and Zhao Y. Tumor microenvironment participates in metastasis of pancreatic cancer. Mol Cancer 2018; 17: 108.

[15] Moffitt RA, Marayati R, Flate EL, Volmar KE, Loeza SG, Hoadley KA, Rashid NU, Williams LA, Eaton SC, Chung AH, Smyla JK, Anderson JM,

Kim HJ, Bentrem DJ, Talamonti MS, Iacobuzio-Donahue CA, Hollingsworth MA and Yeh JJ. Virtual microdissection identifies distinct tumor- and stroma-specific subtypes of pancreatic ductal adenocarcinoma. Nat Genet 2015; 47: 1168-1178.

[16] Whatcott CJ, Diep CH, Jiang P, Watanabe A, LoBello J, Sima C, Hostetter G, Shepard HM, Von Hoff DD and Han H. Desmoplasia in primary tumors and metastatic lesions of pancreatic cancer. Clin Cancer Res 2015; 21: 3561-3568.

[17] Wang X, Lang M, Zhao T, Feng X, Zheng C, Huang C, Hao J, Dong J, Luo L, Li X, Lan C, Yu W, Yu M, Yang S and Ren H. Cancer-FOXP3 directly activated CCL5 to recruit FOXP3(+)Treg cells in pancreatic ductal adenocarcinoma. Oncogene 2017; 36: 3048-3058.

[18] Tang Y, Xu X, Guo S, Zhang C, Tang Y, Tian Y, Ni B, Lu B and Wang H. An increased abundance of tumor-infiltrating regulatory T cells is correlated with the progression and prognosis of pancreatic ductal adenocarcinoma. PLoS One 2014; 9: e91551.

[19] Toole BP. Hyaluronan: from extracellular glue to pericellular cue. Nat Rev Cancer 2004; 4: 528-539.

[20] Itano N, Zhuo L and Kimata K. Impact of the hyaluronan-rich tumor microenvironment on cancer initiation and progression. Cancer Sci 2008; 99: 1720-1725.

[21] Whatcott CJ, Han H, Posner RG, Hostetter G and Von Hoff DD. Targeting the tumor microenvironment in cancer: why hyaluronidase deserves a second look. Cancer Discov 2011; 1: 291-296.

[22] Li XP, Zhang XW, Zheng LZ and Guo WJ. Expression of CD44 in pancreatic cancer and its significance. Int J Clin Exp Pathol 2015; 8: 6724-6731.

[23] Fries H, Elsasser HP, Mahlbacher V, Neumann K and Kern HF. Localisation of hyaluronate (HA) in primary tumors and nude mouse xenografts of human pancreatic carcinomas using a biotinylated HA-binding protein. Virchows Arch 1994; 424: 7-12.

[24] Turley EA, Noble PW and Bourguignon LY. Signaling properties of hyaluronan receptors. J Biol Chem 2002; 277: 4589-4592.

[25] Wu M, Cao M, He Y, Liu Y, Yang C, Du Y, Wang W and Gao F. A novel role of low molecular weight hyaluronan in breast cancer metastasis. FASEB J 2015; 29: 1290-1298.

[26] Schmaus A, Klusmeier S, Rothley M, Dimmler A, Sipos B, Faller G, Thiele W, Allgayer H, Hohenberger P, Post S and Sleeman JP. Accumulation of small hyaluronan oligosaccharides in tumour interstitial fluid correlates with lymphatic invasion and lymph node metastasis. Br J Cancer 2014; 111: 559-567.

[27] Cheng XB, Sato N, Kohi S, Koga A and Hirata K. Receptor for hyaluronic acid-mediated motility is associated with poor survival in pancreatic ductal adenocarcinoma. J Cancer 2015; 6: 1093-1098.

[28] Mahlbacher V, Sewing A, Elsässer HP and Kern HF. Hyaluronan is a secretory product of human pancreatic adenocarcinoma cells. Eur J Cell Biol 1992; 58: 28-34.

[29] McAtee CO, Barycki JJ and Simpson MA. Emerging roles for hyaluronidase in cancer metastasis and therapy. Adv Cancer Res 2014; 123: 1-34.

[30] Kohi S, Sato N, Cheng XB, Koga A and Hirata K. Increased expression of HYAL1 in pancreatic ductal adenocarcinoma. Pancreas 2016; 45: 1467-1473.

[31] Koga A, Sato N, Kohi S, Yabuki K, Cheng XB, Hisaoka M and Hirata K. KIAA1199/CEMIP/HYBID overexpression predicts poor prognosis in pancreatic ductal adenocarcinoma. Pancreatology 2017; 17: 115-122.

[32] Kohi S, Sato N, Koga A, Matayoshi N and Hirata K. KIAA1199 is induced by inflammation and enhances malignant phenotype in pancreatic cancer. Oncotarget 2017; 8: 17156-17163.

[33] Yamamoto H, Tobisawa Y, Inubushi T, Irie F, Ohyama C and Yamaguchi Y. A mammalian homolog of the zebrafish transmembrane protein 2 (TMEM2) is the long-sought-after cell-surface hyaluronidase. J Biol Chem 2017; 292: 7304-7313.

[34] Kobori Y, Tachizaki M, Imaizumi T, Tanaka Y, Seya K, Miki Y, Kawaguchi S, Matsumiya T, Tobisawa Y, Ohyama C and Tasaka S. TMEM2 suppresses TLR3-mediated IFN-β/ISG56/CXCL10 expression in BEAS-2B bronchial epithelial cells. Mol Biol Rep 2024; 51: 417.

[35] De Angelis JE, Lagendijk AK, Chen H, Tromp A, Bower NI, Tunny KA, Brooks AJ, Bakkers J, Francois M, Yap AS, Simons C, Wicking C, Hogan BM and Smith KA. Tmem2 regulates embryonic Vegf signaling by controlling hyaluronic acid turnover. Dev Cell 2017; 40: 123-136.

[36] Chen TC, Wu CL, Lee CC, Chen CL, Yu DS and Huang HS. Structure-based hybridization, synthesis and biological evaluation of novel tetracyclic heterocyclic azathioxanthone analogues as potential antitumor agents. Eur J Med Chem 2015; 103: 615-627.

[37] Madamsetty VS, Pal K, Dutta SK, Wang E, Thompson JR, Banerjee RK, Caulfield TR, Mody K, Yen Y, Mukhopadhyay D and Huang HS. Design and evaluation of PEGylated liposomal formulation of a novel multikinase inhibitor for enhanced chemosensitivity and inhibition of metastatic pancreatic ductal adenocarcinoma. Bioconjug Chem 2019; 30: 2703-2713.

[38] Wu DW, Chen TC, Huang HS and Lee H. TC-N19, a novel dual inhibitor of EGFR and cMET, efficiently overcomes EGFR-TKI resistance in non-small-cell lung cancer cells. Cell Death Dis 2016; 7: e2290.

[39] Wu ATH, Huang HS, Wen YT, Lawal B, Mokgautsi N, Huynh TT, Hsiao M and Wei L. A preclinical investigation of GBM-N019 as a potential inhibitor of glioblastoma via exosomal mTOR/CDK6/STAT3 signaling. Cells 2021; 10: 2391.

[40] Khedkar HN, Wang YC, Yadav VK, Srivastava P, Lawal B, Mokgautsi N, Sumitra MR, Wu ATH and Huang HS. In-silico evaluation of genetic alterations in ovarian carcinoma and therapeutic efficacy of NSC777201, as a novel multi-target agent for TTK, NEK2, and CDK1. Int J Mol Sci 2021; 22: 5895.

[41] Love MI, Huber W and Anders S. Moderated estimation of fold change and dispersion for RNA-seq data with DESeq2. Genome Biol 2014; 15: 550.

[42] Gordon A, Glazko G, Qiu X and Yakovlev A. Control of the mean number of false discoveries, Bonferroni and stability of multiple testing. Ann Appl Stat 2007; 179-190.

[43] Warnes GR, Bolker B, Bonebakker L, Gentleman R, Huber W, Liaw A, Lumley T, Maechler M, Magnusson A and Moeller S. gplots: various R programming tools for plotting data. R Package Version 2009; 2: 1.

[44] Yu G, Wang LG, Han Y and He QY. clusterProfiler: an R package for comparing biological themes among gene clusters. OMICS 2012; 16: 284-287.

[45] Aguirre-Gamboa R, Gomez-Rueda H, Martinez-Ledesma E, Martinez-Torteya A, Chacolla-Huaringa R, Rodriguez-Barrientos A, Tamez-Pena JG and Trevino V. SurvExpress: an online biomarker validation tool and database for cancer gene expression data using survival analysis. PLoS One 2013; 8: e74250.

[46] Robin X, Turck N, Hainard A, Tiberti N, Lisacek F, Sanchez JC and Muller M. pROC: an open-source package for R and S+ to analyze and compare ROC curves. BMC Bioinformatics 2011; 12: 77.

[47] Tran AN, Dussaq AM, Kennell T Jr, Willey CD and Hjelmeland AB. HPAanalyze: an R package that facilitates the retrieval and analysis of the Human Protein Atlas data. BMC Bioinformatics 2019; 20: 463.

[48] Kramer A, Green J, Pollard J Jr and Tugendreich S. Causal analysis approaches in ingenuity pathway analysis. Bioinformatics 2014; 30: 523-530.

[49] Liu Y, Grimm M, Dai WT, Hou MC, Xiao ZX and Cao Y. CB-Dock: a web server for cavity detection-guided protein-ligand blind docking. Acta Pharmacol Sin 2020; 41: 138-144.

[50] Hanwell MD, Curtis DE, Lonie DC, Vandermeersch T, Zurek E and Hutchison GR. Avogadro: an advanced semantic chemical editor, visualization, and analysis platform. J Cheminform 2012; 4: 17.

[51] Visualizer DS. BIOVIA, Dassault Systèmes, BIOVIA Workbook, ReleaseBIOVIA Pipeline Pilot. San Diego, CA: Dassault Systèmes; 2020.

[52] Irie F, Tobisawa Y, Murao A, Yamamoto H, Ohyama C and Yamaguchi Y. The cell surface hyaluronidase TMEM2 regulates cell adhesion and migration via degradation of hyaluronan at focal adhesion sites. J Biol Chem 2021; 296: 100481.

[53] Aier I, Semwal R, Sharma A and Varadwaj PK. A systematic assessment of statistics, risk factors, and underlying features involved in pancreatic cancer. Cancer Epidemiol 2019; 58: 104-110.

[54] Zhao R, Ni J, Lu S, Jiang S, You L, Liu H, Shou J, Zhai C, Zhang W, Shao S, Yang X, Pan H and Han W. CircUBAP2-mediated competing endogenous RNA network modulates tumorigenesis in pancreatic adenocarcinoma. Aging (Albany NY) 2019; 11: 8484-8501.

[55] Wei L, Ye H, Li G, Lu Y, Zhou Q, Zheng S, Lin Q, Liu Y, Li Z and Chen R. Cancer-associated fibroblasts promote progression and gemcitabine resistance via the SDF-1/SATB-1 pathway in pancreatic cancer. Cell Death Dis 2018; 9: 1065.

[56] Kalluri R. The biology and function of fibroblasts in cancer. Nat Rev Cancer 2016; 16: 582-598.

[57] Chen X and Song E. Turning foes to friends: targeting cancer-associated fibroblasts. Nat Rev Drug Discov 2019; 18: 99-115.

[58] Ohlund D, Elyada E and Tuveson D. Fibroblast heterogeneity in the cancer wound. J Exp Med 2014; 211: 1503-1523.

[59] Kudo Y, Sato N, Adachi Y, Amaike T, Koga A, Kohi S, Noguchi H, Nakayama T and Hirata K. Overexpression of transmembrane protein 2 (TMEM2), a novel hyaluronidase, predicts poor prognosis in pancreatic ductal adenocarcinoma. Pancreatology 2020; 20: 1479-1485.

[60] Schmaus A, Bauer J and Sleeman JP. Sugars in the microenvironment: the sticky problem of HA turnover in tumors. Cancer Metastasis Rev 2014; 33: 1059-1079.

[61] Tahkola K, Ahtiainen M, Mecklin JP, Kellokumpu I, Laukkarinen J, Tammi M, Tammi R, Vayrynen JP and Bohm J. Stromal hyaluronan accumulation is associated with low immune response and poor prognosis in pancreatic cancer. Sci Rep 2021; 11: 12216.

[62] Stern R. Hyaluronan catabolism: a new metabolic pathway. Eur J Cell Biol 2004; 83: 317-325.

[63] Yoshida H, Nagaoka A, Kusaka-Kikushima A, Tobiishi M, Kawabata K, Sayo T, Sakai S, Sugiyama Y, Enomoto H, Okada Y and Inoue S. KIAA1199, a deafness gene of unknown function, is a new hyaluronan binding protein involved in hyaluronan depolymerization. Proc Natl Acad Sci U S A 2013; 110: 5612-5617.

[64] Sato N, Kohi S, Hirata K and Goggins M. Role of hyaluronan in pancreatic cancer biology and therapy: once again in the spotlight. Cancer Sci 2016; 107: 569-575.

[65] Lee H, Goodarzi H, Tavazoie SF and Alarcón CR. TMEM2 is a SOX4-regulated gene that mediates metastatic migration and invasion in breast cancer. Cancer Res 2016; 76: 4994-5005.

[66] Jiang Q, Wang X, Yang Q, Zhang H and Wang X. *TMEM2* combined with *IDH* and 1p19q in refining molecular subtypes for predicting survival of patients with glioma. DNA Cell Biol 2021; 40: 1381-1395.

[67] Gan L, Yang H, Xiong Z, Yang Z, Wang T and Lyu G. miR-518a-3p suppresses triple-negative breast cancer invasion and migration through regulation of TMEM2. Technol Cancer Res Treat 2020; 19: 1533033820977523.

[68] Waghray M, Yalamanchili M, di Magliano MP and Simeone DM. Deciphering the role of stroma in pancreatic cancer. Curr Opin Gastroenterol 2013; 29: 537-543.

[69] Vennin C, Murphy KJ, Morton JP, Cox TR, Pajic M and Timpson P. Reshaping the tumor stroma for treatment of pancreatic cancer. Gastroenterology 2018; 154: 820-838.

[70] Sahai E, Astsaturov I, Cukierman E, DeNardo DG, Egeblad M, Evans RM, Fearon D, Greten FR, Hingorani SR, Hunter T, Hynes RO, Jain RK, Janowitz T, Jorgensen C, Kimmelman AC, Kolonin MG, Maki RG, Powers RS, Pure E, Ramirez DC, Scherz-Shouval R, Sherman MH, Stewart S, Tlsty TD, Tuveson DA, Watt FM, Weaver V, Weeraratna AT and Werb Z. A framework for advancing our understanding of cancer-associated fibroblasts. Nat Rev Cancer 2020; 20: 174-186.

[71] Ungefroren H, Groth S, Sebens S, Lehnert H, Gieseler F and Fandrich F. Differential roles of Smad2 and Smad3 in the regulation of TGF-beta1-mediated growth inhibition and cell migration in pancreatic ductal adenocarcinoma cells: control by Rac1. Mol Cancer 2011; 10: 67.

[72] Yamaguchi T, Ikehara S, Akimoto Y, Nakanishi H, Kume M, Yamamoto K, Ohara O and Ikehara Y. TGF-beta signaling promotes tube-structure-forming growth in pancreatic duct adenocarcinoma. Sci Rep 2019; 9: 11247.

[73] McCarthy JB, El-Ashry D and Turley EA. Hyaluronan, cancer-associated fibroblasts and the tumor microenvironment in malignant progression. Front Cell Dev Biol 2018; 6: 48.
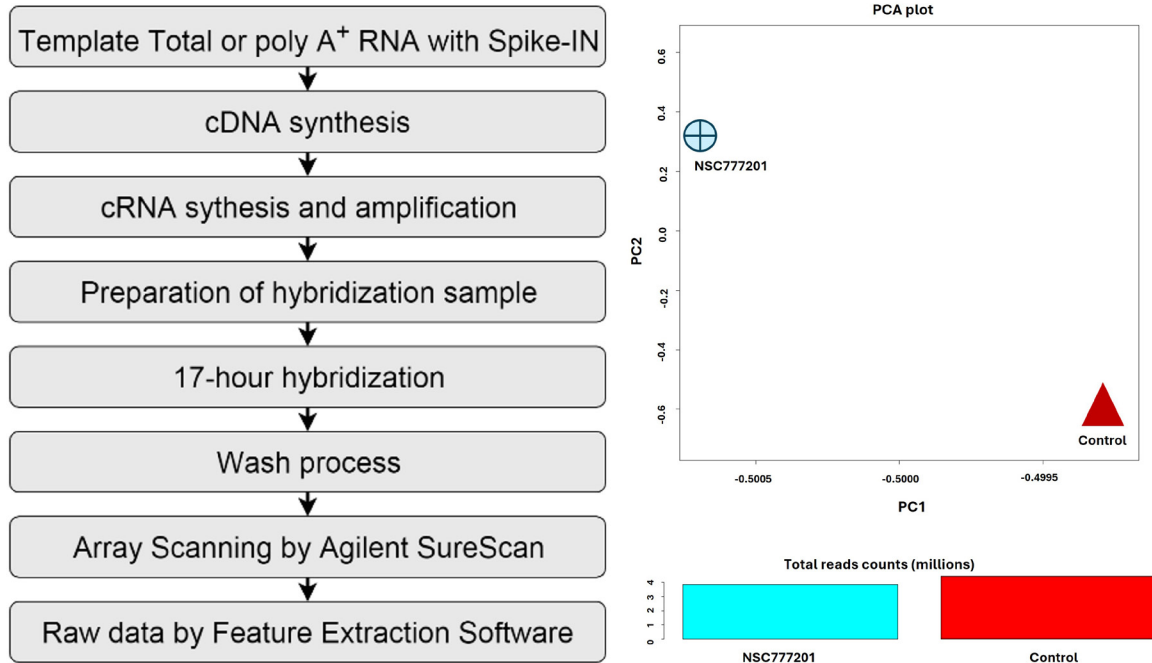
Figure S1. Experimental flow of microarray sequencing. NSC777201 treated Panc1 cells, right panel showing the PCA and total read counts (million).

Table S1. Primer details

Gene symbol	Forward	Reverse
TWIST1	CGGGAGTCCGCAGTCTTA	CTTGAGGGTCTGAATCTTGCT
GAPDH	CATCATCCCTGCCTCTACTG	GCCTGCTTCACCACCTTC
SNAI	TTCTTCTGCGCTACTGCTGCG	GGGCAGGTATGGAGAGGAAGA
Zeb1	TTCACAGTGGAGAGAAGCCA	GCCTGGTGATGCTGAAAGAG
TMEM2	TCCACAGTACCAGCCTGTCGTC	TGATGGATAGCAAAGGCCAACTC
FN1	GTGTGACCCTCATGAGGCAAC	CTGGCCTCCAAAGCATGTG
FAP	TGCTCTCTGGTGGTCTCCTAA	TTAGGAGACCACCAGAGAGCA
αSMA	GTGACTACTGCCGAGCGTG	ATAGGTGGTTTCGTGGATGC

List of Antibodies			
Target	Dilution	Company and Catalog No.	Predicted MW (kDa)
GAPDH	1:1000	Proteintech, IL6 Rabbit mAb, 10494-1-AP	36
FAP	1:500	Anti-Fibroblast activation protein, alpha antibody (Adcam, ab53066)	≈90
TMEM2	1:500	Rabbit polyclonal anti-Tmem2 (Abcam, ab272644)	≈154

Table S2. Details for GEO normal fibroblast (NFs) and cancer-associated fibroblast (CAFs)

Sample	GEO	Platform	CAFs	NFs
Human Pancreatic Ductal Adenocarcinoma	GSE172096	GPL24676	5	3

1

Table S3. A total of 416-DEGs between CAFs and NFs samples

DEGs-CAFs	log2Fold Change	Adj.Pval	DEGs-CAFs	log2Fold Change	Adj.Pval
SMYD3	25.01387	7.75E-10	SCAMP1	22.75684	7.99E-10
CSGALNACT2	24.34192	7.75E-10	SETDB1	22.75684	7.99E-10
AL121957.1	24.33809	7.75E-10	USP3	22.75684	7.99E-10
DNAJC6	24.2185	7.75E-10	AF230666.1	22.70137	8.28E-10
TEX9	24.18985	7.75E-10	ANKRD44	22.70137	8.28E-10
RAB7A	23.85294	7.75E-10	B4GALT6	22.70137	8.28E-10
HAT1	23.82339	7.75E-10	CPED1	22.70137	8.28E-10
FANCM	23.81842	7.75E-10	EIF3E	22.70137	8.28E-10
NR3C2	23.78796	7.75E-10	ETV6	22.70137	8.28E-10
VPS13A	23.78796	7.75E-10	FBXO4	22.70137	8.28E-10
ZFC3H1	23.77166	7.75E-10	GGNBP2	22.70137	8.28E-10
SPAG16	23.7402	7.75E-10	MICAL2	22.70137	8.28E-10
ACSS3	23.73395	7.75E-10	OBSCN	22.70137	8.28E-10
RFX8	23.73135	7.75E-10	PPP2R3C	22.70137	8.28E-10
GRAMD4	23.71861	7.75E-10	REPS1	22.70137	8.28E-10
KLHDC10	23.70673	7.75E-10	TBC1D14	22.70137	8.28E-10
CAMSAP1	23.70254	7.75E-10	TRNT1	22.70137	8.28E-10
SMURF2	23.69846	7.75E-10	YARS	22.70137	8.28E-10
STX16	23.67373	7.75E-10	AC010877.1	22.64071	8.81E-10
ECSIT	23.66121	7.75E-10	AMBRA1	22.64071	8.81E-10
SOCS7	23.66121	7.75E-10	DEAF1	22.64071	8.81E-10
INO80	23.61116	7.75E-10	HMBOX1	22.64071	8.81E-10
FANCB	23.59646	7.75E-10	RASA2	22.64071	8.81E-10
SPTLC1P1	23.59646	7.75E-10	SAMD3	22.64071	8.81E-10
DTL	23.59524	7.75E-10	SNORD67	22.64071	8.81E-10
KIF23	23.57526	7.75E-10	TBC1D23	22.64071	8.81E-10
NEK7	23.57526	7.75E-10	UBE2D2	22.64071	8.81E-10
BPTF	23.56856	7.75E-10	SDF4	22.62686	8.81E-10
RN7SL274P	23.56856	7.75E-10	AC109357.1	22.62437	8.81E-10
TXNRD1	23.56608	7.75E-10	CAP2	22.62437	8.81E-10
SPRYD7	23.5384	7.75E-10	DNAJC11	22.62437	8.81E-10
UBR5	23.53013	7.75E-10	FUT10	22.62437	8.81E-10
UBXN7	23.53013	7.75E-10	HIVEP1	22.62437	8.81E-10
TMEM50A	23.51335	7.75E-10	PAPPA2	22.62437	8.81E-10
MAP2K4	23.50901	7.75E-10	PFKFB3	22.62437	8.81E-10
ARHGEF7	23.49636	7.75E-10	PPP6R3	22.62437	8.81E-10
GLIS1	23.49556	7.75E-10	TRA2B	22.62437	8.81E-10
USP42	23.49556	7.75E-10	KMT2A	22.5374	1.02E-09
EPHA3	23.47613	7.75E-10	SATB1	22.5374	1.02E-09
SSFA2	23.47613	7.75E-10	AGTPBP1	22.28516	1.62E-09
HEXB	23.44897	7.75E-10	PDGFC	22.28516	1.62E-09
NEDD9	23.44233	7.75E-10	GPRC5B	22.16796	1.98E-09
EMILIN2	23.43549	7.75E-10	MAST2	22.16796	1.98E-09
RNF34	23.43549	7.75E-10	TRAPPC10	22.16796	1.98E-09
TNIK	23.42842	7.75E-10	PAPPA-AS2	21.41577	7.55E-09
ASPHD1	23.40569	7.75E-10	MAN1A2	11.25015	5.57E-06
CENPJ	23.40569	7.75E-10	FARP1	11.06933	3.15E-04

INTS2	23.40569	7.75E-10	SH2B3	10.8502	2.86E-03
UBE3C	23.39986	7.75E-10	AXIN1	10.83193	4.65E-04
EZH2	23.37726	7.75E-10	AC092120.2	10.80317	3.33E-03
PRKAA1	23.37726	7.75E-10	RACGAP1	10.80215	2.98E-03
WDHD1	23.37726	7.75E-10	ABR	10.73675	5.44E-04
EPB41L2	23.36872	7.75E-10	UBE4B	10.65121	5.96E-04
PDE5A	23.36872	7.75E-10	TIPARP	10.64713	3.78E-03
AKAP11	23.34952	7.75E-10	SNORA30	10.6233	3.22E-05
FASTKD1	23.34952	7.75E-10	RNU4-49P	10.55894	7.28E-04
CCDC88A	23.34709	7.75E-10	SNX11	10.53953	7.66E-04
MCTP2	23.34709	7.75E-10	OXSR1	10.51687	7.54E-04
LTBP4	23.33551	7.75E-10	AC092964.2	10.48283	8.21E-04
RABGAP1	23.33551	7.75E-10	DNAJC1	10.4059	5.04E-03
EXOC2	23.33069	7.75E-10	LONP2	10.40076	5.13E-03
MBTD1	23.31335	7.75E-10	ST3GAL3	10.2896	5.93E-03
ATP2A2	23.30135	7.75E-10	DUTP7	10.28667	6.07E-03
SEC63P1	23.30135	7.75E-10	MPP6	10.28017	1.20E-03
UBXN2A	23.30135	7.75E-10	SNHG12	10.27925	6.28E-03
YTHDF1	23.30135	7.75E-10	COG2	10.16562	6.89E-03
NFATC1	23.29841	7.75E-10	LHFPL2	10.15856	1.40E-03
TNRC18	23.29841	7.75E-10	RNF4	10.12508	7.21E-03
ALPK2	23.29058	7.75E-10	GPR137B	10.12054	7.35E-03
KDSR	23.29058	7.75E-10	EHMT1	10.11904	7.35E-03
MCM9	23.29058	7.75E-10	OXCT1	10.10595	7.27E-03
Y_RNA	23.29058	7.75E-10	RN7SL859P	10.1042	7.24E-03
ZNF131	23.29058	7.75E-10	CDC5L	10.03804	7.83E-03
MEIS1	23.28401	7.75E-10	ASCC2	10.03477	7.83E-03
PHF12	23.28401	7.75E-10	CUL2	10.02087	1.75E-03
STK40	23.28401	7.75E-10	AKAP13	10.01298	7.94E-03
LACTB	23.27089	7.75E-10	DIAPH3	10.01298	7.94E-03
UBLCP1	23.24189	7.75E-10	DIDO1	9.990334	8.15E-03
ZNF280D	23.22846	7.75E-10	NCAPG	9.98226	8.20E-03
SH3RF3	23.2132	7.75E-10	PIKFYVE	9.941067	8.77E-03
AC007738.1	23.20748	7.75E-10	EXOC5	9.933992	8.81E-03
DCBLD1	23.20748	7.75E-10	LINC02246	9.927544	9.10E-03
HNRNPA3P9	23.20748	7.75E-10	PRUNE1	9.925649	8.86E-03
NSD2	23.20238	7.75E-10	APLP2	9.922578	8.96E-03
TPX2	23.2022	7.75E-10	FNIP2	9.873974	9.30E-03
ATRNL1	23.19823	7.75E-10	CEP128	9.859862	9.36E-03
GAS2L3	23.19823	7.75E-10	PHF20	9.85792	9.52E-03
PPP3CA	23.17773	7.75E-10	FLVCR2	9.834658	9.78E-03
SLC39A10	23.17773	7.75E-10	NAA25	9.812982	1.01E-02
CBLB	23.16124	7.75E-10	EEFSEC	9.81125	1.00E-02
GAREM1	23.16124	7.75E-10	ELF2	9.807385	2.62E-03
PSMD9	23.16124	7.75E-10	FAM114A2	9.790662	1.01E-02
EIF3B	23.1442	7.75E-10	FNIP1	9.787186	1.01E-02
TGFBR2	23.1442	7.75E-10	ALAS1	9.781685	1.01E-02
ADGRE5	23.13046	7.75E-10	NPRL3	9.781685	1.01E-02
DOK5	23.13046	7.75E-10	RN7SL373P	9.781685	1.01E-02

TMEM44	23.13046	7.75E-10	TRAM1	9.781199	1.03E-02
AC004076.1	23.10926	7.75E-10	AC134407.1	9.774134	1.03E-02
ANKH	23.10926	7.75E-10	SEL1L3	9.76078	1.05E-02
G3BP1	23.10926	7.75E-10	RABGEF1	9.752848	1.03E-02
NEK9	23.10926	7.75E-10	NR4A3	9.747452	1.07E-02
RNA5SP425	23.10926	7.75E-10	AC011462.1	9.739929	1.08E-02
EPSTI1	23.0563	7.75E-10	DOCK6	9.72205	1.07E-02
KIAA0355	23.0563	7.75E-10	EIF3H	9.708308	1.10E-02
MIR491	23.0563	7.75E-10	SAP130	9.69278	1.13E-02
BRF1	23.02214	7.75E-10	MOV10L1	9.664536	1.14E-02
C17ORF53	23.02214	7.75E-10	ZNF644	9.664536	1.14E-02
EXOC6	23.02214	7.75E-10	XRN2	9.658455	1.17E-02
KREMEN1	23.02214	7.75E-10	RAB1A	9.623386	1.21E-02
MGLL	23.02214	7.75E-10	TTBK2	9.623386	1.21E-02
ATG16L1	23.01689	7.75E-10	CKAP5	9.593382	1.25E-02
DDX6	23.01689	7.75E-10	MIR548S	9.580768	1.26E-02
NAA15	23.01689	7.75E-10	ZNF418	9.580768	1.26E-02
ZNF585B	23.01689	7.75E-10	ACOX1	9.57647	1.27E-02
PPP1R12C	22.99368	7.75E-10	STX12	9.556675	1.29E-02
AL133243.1	22.94855	7.75E-10	AC006529.1	9.505354	1.34E-02
GAN	22.94855	7.75E-10	SIPA1L3	9.498949	1.38E-02
RNU6-1026P	22.94855	7.75E-10	AC130472.1	9.494114	1.36E-02
GNAZ	22.94517	7.75E-10	LRPPRC	9.459615	1.46E-02
ANO10	22.9348	7.75E-10	SIAE	9.459615	1.46E-02
ARHGEF12	22.9348	7.75E-10	TAF4	9.459615	1.46E-02
ZDHHC5	22.9348	7.75E-10	TMEM2	9.447717	1.46E-02
ATL3	22.9179	7.75E-10	MAPK8	9.426082	1.47E-02
KATNAL1	22.9179	7.75E-10	MBD2	9.426082	1.47E-02
MYCBP2	22.9179	7.75E-10	ADD1	9.377405	1.52E-02
PPP1R21	22.9179	7.75E-10	RETSAT	9.28805	1.72E-02
PRPSAP2	22.9179	7.75E-10	BRAP	9.274975	1.74E-02
AURKA	22.90923	7.75E-10	C9ORF3	9.274975	1.74E-02
CDKN2B-AS1	22.90923	7.75E-10	SAFB	9.274975	1.74E-02
CHD1	22.90923	7.75E-10	C1ORF132	9.220813	1.88E-02
COX5A	22.90923	7.75E-10	SNORD90	9.220813	1.88E-02
GRIN2D	22.90923	7.75E-10	PBX3	-10.7421	3.86E-03
PDS5B	22.90923	7.75E-10	N4BP2L2	-10.6985	4.01E-03
PGD	22.90923	7.75E-10	SLC35F5	-10.6985	4.01E-03
PHLPP2	22.90923	7.75E-10	DTWD1	-10.6917	3.97E-04
PKD2	22.90923	7.75E-10	NEK1	-10.6267	4.73E-04
PRPF39	22.90923	7.75E-10	MDN1	-10.6223	5.06E-04
SNX7	22.90923	7.75E-10	ATG4C	-10.5692	5.04E-03
TMEM106B	22.90923	7.75E-10	TANGO6	-10.5552	5.04E-03
TMOD3	22.90923	7.75E-10	DGKI	-10.4953	5.62E-03
TOLLIP	22.90923	7.75E-10	MFAP5	-10.4953	5.62E-03
ZDHHC17	22.90923	7.75E-10	BRWD1	-10.4805	5.68E-03
AL049872.1	22.90628	7.75E-10	ATP6V0A1	-10.4218	6.16E-03
KLHL28	22.90628	7.75E-10	ANKRD13C	-10.4168	8.04E-04
NOL10	22.90628	7.75E-10	PAN3	-10.4168	8.04E-04
TULP4	22.90628	7.75E-10	ZDHHC4	-10.4092	6.29E-03

UBAP2L	22.90628	7.75E-10	STXBP5	-10.3467	7.02E-03
AKAP9	22.88944	7.75E-10	AL390774.1	-10.3432	7.04E-03
ERICH1	22.88944	7.75E-10	ZNF407	-10.3391	7.05E-03
FBXO11	22.88944	7.75E-10	KCNK2	-10.2614	7.82E-03
FOXK1	22.88944	7.75E-10	RNU6-1297P	-10.2473	7.94E-03
KAT6A	22.88944	7.75E-10	SENP6	-10.2473	7.94E-03
MED13L	22.88944	7.75E-10	KAT6B	-10.1731	8.85E-03
MTRF1	22.88944	7.75E-10	PRCP	-10.1671	1.45E-03
MYO1E	22.88944	7.75E-10	RNF19A	-10.1671	1.45E-03
NDST1	22.88944	7.75E-10	SNORA23	-10.1571	9.21E-03
PLPP4	22.88944	7.75E-10	USP45	-10.1571	9.21E-03
SEC22A	22.88944	7.75E-10	MYO9A	-10.0834	9.99E-03
TRIP12	22.88944	7.75E-10	CNOT7	-10.0743	1.01E-02
FAM192A	22.85947	7.75E-10	AL121893.1	-10.0674	1.01E-02
HMGCL	22.85947	7.75E-10	RNU6-74P	-10.0674	1.01E-02
TUSC3	22.85947	7.75E-10	DENND1B	-9.98035	1.12E-02
USP7	22.85947	7.75E-10	LAMA2	-9.98035	1.12E-02
AC092902.2	22.84862	7.75E-10	WDR70	-9.98035	1.12E-02
BMP2K	22.84862	7.75E-10	CCNE2	-9.96895	1.14E-02
MRC2	22.84862	7.75E-10	SBF2	-9.96895	1.14E-02
PRTFDC1	22.84862	7.75E-10	ETS1	-9.87727	1.30E-02
SHANK2	22.84862	7.75E-10	ISPD-AS1	-9.87727	1.30E-02
SLC8B1	22.84862	7.75E-10	REV3L	-9.87727	1.30E-02
EXOC4	22.84659	7.75E-10	KLF7	-9.85885	1.33E-02
KIF3B	22.84659	7.75E-10	RGS12	-9.85885	1.33E-02
SAMD8	22.84659	7.75E-10	SHPRH	-9.85885	1.33E-02
ST7-AS2	22.84659	7.75E-10	ALG8	-9.76103	1.47E-02
TMEM120B	22.84659	7.75E-10	CDKAL1	-9.76103	1.47E-02
TRRAP	22.84659	7.75E-10	ENAH	-9.76103	1.47E-02
YEATS2	22.84659	7.75E-10	LDAH	-9.76103	1.47E-02
AC020915.6	22.84365	7.75E-10	NDUFS3	-9.76103	1.47E-02
AC026474.1	22.84365	7.75E-10	RASA2-IT1	-9.76103	1.47E-02
AC104662.2	22.84365	7.75E-10	SSR1	-9.76103	1.47E-02
AFF4	22.84365	7.75E-10	USP49	-9.76103	1.47E-02
GRB10	22.84365	7.75E-10	ARFGEF1	-9.74974	1.47E-02
NALCN	22.84365	7.75E-10	ATP9A	-9.74974	1.47E-02
SMAD1	22.84365	7.75E-10	DDX59	-9.74974	1.47E-02
TOX2	22.84365	7.75E-10	RNU6-836P	-9.74974	1.47E-02
ZC3H14	22.84365	7.75E-10	AL033529.1	-9.74774	1.47E-02
AC093732.2	22.80656	7.80E-10	AL513365.1	-9.74774	1.47E-02
AC104791.2	22.80656	7.80E-10	ARHGEF10	-9.74774	1.47E-02
CFLAR	22.80656	7.80E-10	C16ORF72	-9.74774	1.47E-02
DDX23	22.80656	7.80E-10	CHFR	-9.74774	1.47E-02
FIG4	22.80656	7.80E-10	KIAA1958	-9.74774	1.47E-02
HELZ	22.80656	7.80E-10	ME2	-9.74774	1.47E-02
IBTK	22.80656	7.80E-10	ARMC8	-9.49839	2.04E-02
KIF14	22.80656	7.80E-10	ASAP1-IT2	-9.49839	2.04E-02
LRRC41	22.80656	7.80E-10	BRAF	-9.49839	2.04E-02
NANS	22.80656	7.80E-10	D2HGDH	-9.49839	2.04E-02

TMEM2 in pancreatic cancer: biomarker analysis & NSC777201 drug potential

SPG11	22.80656	7.80E-10	DNAJC16	-9.49839	2.04E-02
UBN2	22.80656	7.80E-10	MEG8	-9.49839	2.04E-02
AURKB	22.75684	7.99E-10	MYO1D	-9.49839	2.04E-02
CCDC138	22.75684	7.99E-10	PIBF1	-9.49839	2.04E-02
CLOCK	22.75684	7.99E-10	PRMT2	-9.49839	2.04E-02
DLAT	22.75684	7.99E-10	SMCHD1	-9.49839	2.04E-02
HERC2	22.75684	7.99E-10	AC093142.1	-9.48243	2.04E-02
HNRNPUL2-BSCL2	22.75684	7.99E-10	ATAD2	-9.48243	2.04E-02
LATS2	22.75684	7.99E-10	DONSON	-9.48243	2.04E-02
LRCH3	22.75684	7.99E-10	ITGBL1	-9.48243	2.04E-02
MARK3	22.75684	7.99E-10	PSMD5	-9.48243	2.04E-02
NUP35	22.75684	7.99E-10	RNU6-720P	-9.48243	2.04E-02
RN7SL851P	22.75684	7.99E-10	Z99496.1	-9.48243	2.04E-02
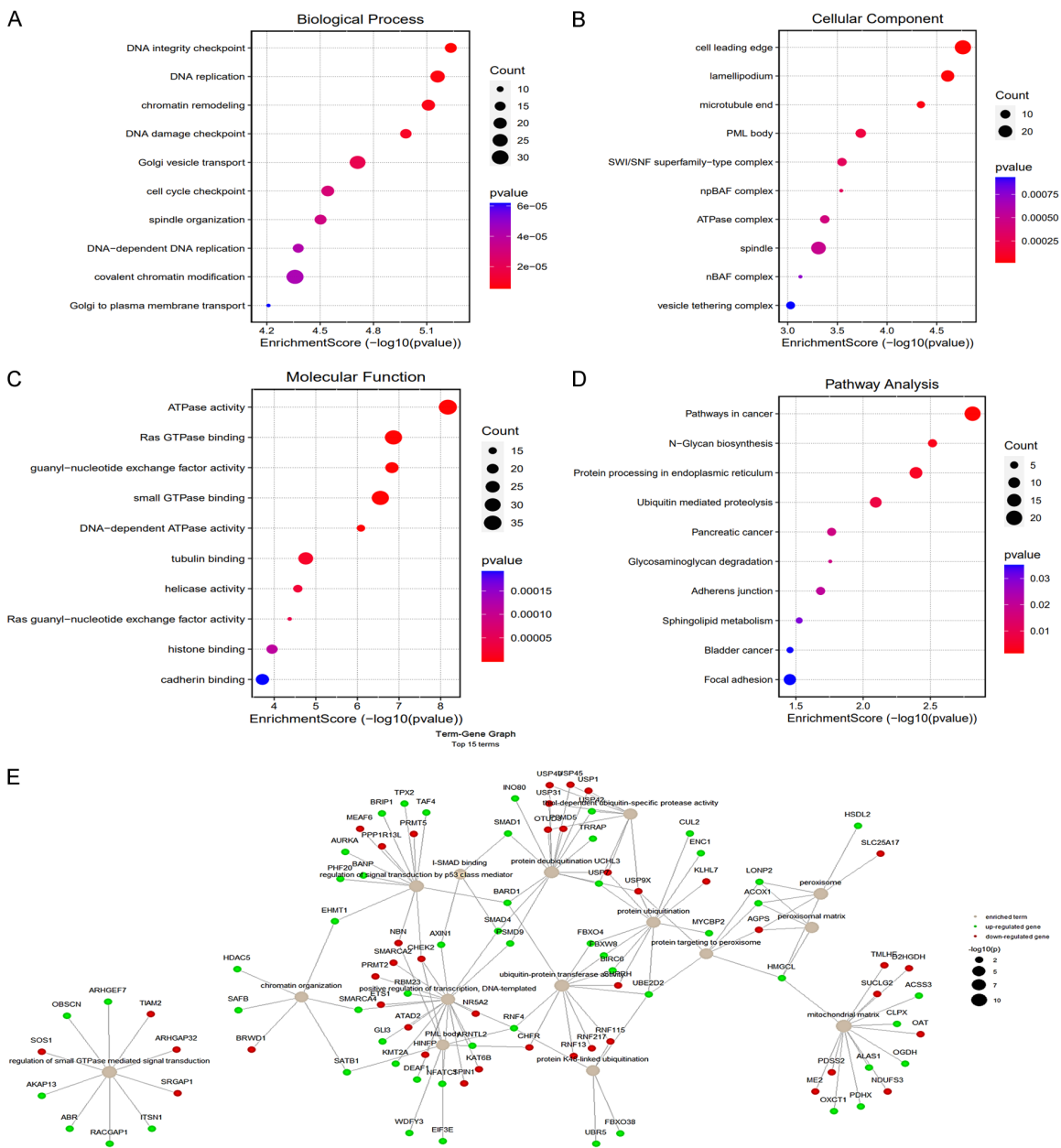
Figure S2. Dotplots of the gene ontology (GO) analysis and Kyoto Encyclopaedia of Genes and Genomes (KEGG) pathway analysis, overrepresented with a -log10 *p*-value threshold of <0.05 in the sets of CAFs-DEGs. (A-C) GO-biological process (BP), cellular component (CC) and Molecular Function (MF) of DEGs according to the -log10 *p* value for each GO term, (D) KEGG pathway analysis of DEGs, with the top 10 pathway. (E) Cnet plot representing GO-All terms and the associated genes commonly up/or downregulated in the DEGs.

A

SwissADME

SwissADME	NSC777201	SwissADME	Molecule 1
Canonical SMILES	OCCNCCCNc1nc2ccccc2c2c1sc1ccc(cc1c2=O)Cl	Ali Class	Poorly soluble
Formula	C21H20ClN3O2S	Silicos-IT LogSw	-8.72
MW	413.92	Silicos-IT Solubility (mg/ml)	7.81E-07
#Heavy atoms	28	Silicos-IT Solubility (mol/l)	1.89E-09
#Aromatic heavy atoms	18	Silicos-IT class	Poorly soluble
Fraction Csp3	0.24	GI absorption	High
#Rotatable bonds	7	BBB permeant	No
#H-bond acceptors	4	Pgp substrate	Yes
#H-bond donors	3	CYP1A2 inhibitor	Yes
MR	118.41	CYP2C19 inhibitor	Yes
TPSA	102.49	CYP2C9 inhibitor	Yes
iLOGP	3.47	CYP2D6 inhibitor	Yes
XLOGP3	4.51	CYP3A4 inhibitor	Yes
WLOGP	3.81	log Kp (cm/s)	-5.62
MLOGP	2.68	*Lipinski #violations*	0
Silicos-IT Log P	5.63	*Ghose #violations*	*0*
Consensus Log P	4.02	*Veber #violations*	*0*
ESOL Log S	-5.26	*Egan #violations*	*0*
ESOL Solubility (mg/ml)	2.27E-03	*Muegge #violations*	*0*
ESOL Solubility (mol/l)	5.48E-06	*Bioavailability Score*	*0.55*
ESOL Class	Moderately soluble	*PAINS #alerts*	*0*
Ali Log S	-6.38	*Brenk #alerts*	*2*
Ali Solubility (mg/ml)	1.71E-04	*Leadlikeness #violations*	*2*
Ali Solubility (mol/l)	4.14E-07	*Synthetic Accessibility*	*3.26*

B

ADMETlab2.0E

ADMETlab 2.0	NSC777201	ADMETlab 2.0	NSC777201	ADMETlab 2.0	NSC777201	ADMETlab 2.0	NSC777201
LogS	-4.321	NR-Aromatase	0.943	CYP3A4-sub	0.505	Toxicophores	2
LogD	2.783	NR-ER	0.233	CL	4.649	Acute_Aquatic_Toxicity	1
LogP	3.8	NR-ER-LBD	0.319	T12	0.074	LD50_oral	0
Pgp-inh	0.071	NR-PPAR-gamma	0.752	hERG	0.88	NonGenotoxic_Carcinogenicity	2
Pgp-sub	1	SR-ARE	0.922	H-HT	0.947	Skin_Sensitization	0
HIA	0.004	SR-ATAD5	0.92	DILI	0.947	SureChEMBL	0
F(20%)	0.003	SR-HSE	0.155	Ames	0.555	Genotoxic_Carcinogenicity_Mutagenicity	3
F(30%)	0.511	SR-MMP	0.839	ROA	0.699	NonBiodegradable	2
Caco-2	-5.501	SR-p53	0.965	FDAMDD	0.887	QED	0.257
MDCK	1.78E-05	MW	413.1	SkinSen	0.922	Synth	2.953
BBB	0.487	Vol	398.109	Carcinogenicity	0.039	Fsp3	0.238
PPB	84.51%	Dense	1.038	EC	0.005	MCE-18	21
VDss	2.451	nHA	5	EI	0.051	Natural Product-likeness	-0.527
Fu	10.74%	nHD	3	Respiratory	0.945	Alarm_NMR	1
CYP1A2-inh	0.95	TPSA	77.48	BCF	1.394	BMS	1
CYP1A2-sub	0.384	nRot	6	IGC50	4.794	Chelating	0
CYP2C19-inh	0.488	nRing	4	LC50	5.212	PAINS	0
CYP2C19-sub	0.092	MaxRing	18	LC50DM	5.836	*Lipinski*	*Accepted*
CYP2C9-inh	0.037	nHet	7	NR-AR	0.005	*Pfizer*	*Accepted*
CYP2C9-sub	0.075	fChar	0	NR-AR-LBD	0.837	*GSK*	*Rejected*
CYP2D6-inh	0.944	nRig	23	NR-AhR	0.988	*GoldenTriangle*	*Accepted*
CYP2D6-sub	0.45	Flex	0.261				
CYP3A4-inh	0.499	nStereo	0				

Figure S3. NSC777201 passed the required drug-likeness criteria. A. SwissADME webserver, demonstrate NSC777201 pass the drug-likeness properties according to Lipinski (Pfizer), Ghose (Amgen), Veber (GSK), Egan (Pharmacia) criteria, furthermore, the relationship between the PK and physiochemical properties, and Gastrointestinal absorption (high), bioavailability score (55%) all demonstrated NSC777201 towards a lead drug. B. ADMETlab2.0 webserver also, demonstrate NSC777201 pass the drug-likeness properties according to Lipinski, Pfizer, and golden triangle (favorable ADMET profile) all demonstrated NSC777201 towards a lead drug.
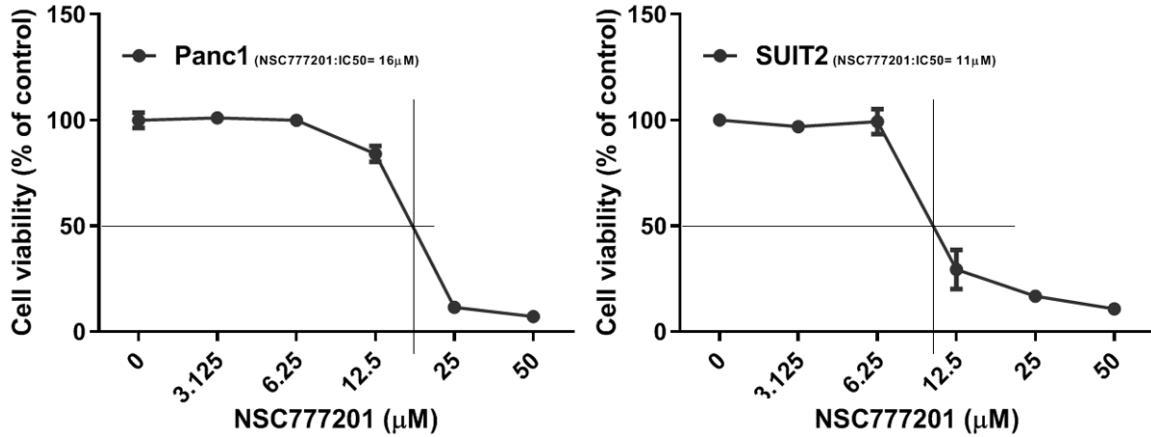
Figure S4. SRB assays. Cell viability assay showed that effect of NSC77201 on the Panc1 and Suit2 cells, for IC50 estimation.

Table S4. A total of 570-DEGs between NSC7777201 vs. Control Panc1 cells

NSC7777201-DEGS	log2FC	NSC7777201-DEGS	log2FC	NSC7777201-DEGS	log2FC
VLDLR-AS1	1.24687916	TDRKH	1.31856301	C17orf59	1.630754073
LINC00662	1.24017088	CYR61	-1.5082192	WBP2	1.230599639
H19	-1.4705876	YIF1A	1.27014673	C2orf44	-1.27538834
LOC400958	2.66620475	HSD17B12	1.22903351	TUBA4A	-1.27947366
CASC15	2.90020066	UCP2	1.29252178	CYTH4	-1.86892527
ATF7IP2	-1.8519824	TMEM55B	1.4293559	SEC24D	1.417614154
C16orf52	-1.404814	RAD51D	-1.206467	FOSL1	-1.45449247
PGM3	1.31502951	FYN	1.58918776	POLE2	-1.22778565
USB1	-1.2791926	FTL	1.28599307	C15orf52	-1.39367495
SCARNA22	1.50125416	RAMP1	1.4781881	KLHL23	-1.28036105
SNORA84	1.2715127	GBP3	-2.2171828	ENST00000407780	-1.24959064
SNAR-G1	-1.4984502	GRHL3	-1.918104	TMEM191A	1.252079076
SNAR-F	-1.3110397	NAV2	-1.5883802	VOPP1	-1.26107839
VTRNA1-2	1.42313812	SYTL2	-1.3247728	TP53INP1	1.885328954
VTRNA1-3	1.55158174	COG6	1.48431037	OPLAH	1.224732294
HIVEP3	-1.3014034	HERPUD1	2.40681983	CD82	-1.72405366
OSER1-AS1	1.56401791	LDHD	2.43121241	PNPLA3	1.202305508
LOC102723817	-1.5809004	NR1H2	1.3197813	ARSI	-1.52444557
lnc-HMCN1-2	3.05502918	MCEE	1.69582498	PGM3	1.381294412
ENST00000450667	3.02302011	CLDN1	-1.2739474	CTGF	-1.38837612
lnc-AC069257.9.1-5	-1.2523634	S100P	3.14167096	NEXN	-1.90799269
ENST00000507681	2.26491667	EPB41L4A-AS1	1.60891534	DDAH1	-1.73092453
lnc-SUPT3H-1	2.90791363	ZSWIM1	-2.200969	LAMC2	-1.3457245
LINC01186	-1.772479	MSTO1	1.45473529	CASP1	-1.76979726
lnc-RPP30-2	2.84585637	RHBDL2	-2.7849443	SSPN	-1.22300307
ENST00000561588	-2.5305088	SDF2L1	1.25406635	AACS	1.720245073
lnc-SOX6-1	3.00843686	FAM213A	1.36738663	CDKN1B	1.275121677
lnc-HNF1A-1	2.35359123	KIAA1549L	-1.7473898	ASB2	-1.95675669
lnc-FSCN2-1	-1.3178053	CPAMD8	1.2079724	ABHD4	1.834624077
WFDC21P	2.41398658	GALM	1.23716376	TPM1	-1.23713688
PDCD6IPP2	1.58680394	MCM8	-1.3159709	FANCA	-1.31672571

XLOC_l2_005692	1.37615904	FAT1	-1.4511801	MAP3K14	-1.25247815
ENST00000589038	1.59426804	CD83	-2.1214997	CDK20	1.364410034
ENST00000451884	-1.4007933	ZCWPW1	1.47332692	TNS4	-1.50627503
ANKRD20A9P	-1.2495126	FDFT1	1.35543183	UHRF1	-1.39084658
ANKRD20A11P	-1.2513248	CXCL1	-1.4505418	LGALSL	1.638303988
TMEM191B	1.25649932	RAD54L	-1.2661007	TRIB3	2.063999576
EVA1C	-1.3836963	G0S2	-2.0982136	ACSS2	3.392013775
XLOC_l2_011118	-1.431938	C1orf54	2.29083998	LSS	2.228177757
ENST00000511103	1.53981477	KIF20B	-1.3566045	DDIT3	3.875605099
ENST00000518311	1.2505272	LHPP	1.42230558	TGFBR2	-1.23039432
XLOC_l2_014549	1.29556542	RAB3IL1	1.7572553	FSTL1	-1.23545954
ENST00000402318	-1.3055882	SLC3A2	1.99887933	CBLB	1.45083732
LOC388813	8.65104273	IL23A	2.47193961	F2R	-1.36863871
LOC100507291	1.75947127	EMP1	-1.4905606	EGR1	1.356259278
THC2690033	-1.3716116	GALNT16	-1.4231765	ZSCAN31	1.87827994
GACAT2	1.78594967	OSGIN1	2.78534008	PODXL	-1.23783697
A_21_P0014880	1.71803148	MAP1LC3B	1.20892294	POLQ	-1.35131123
DGUOK-AS1	-1.2610377	FAM117A	1.94190364	GNL3L	-1.36403634
lnc-C3orf52-1	-1.5069994	ALDOC	1.67386995	ARMCX1	1.212258797
lnc-DBN1-2	-1.2856804	UBD	-1.6274675	PINK1	1.42223248
ERN1	1.33809826	ME1	1.64850002	EXO1	-1.63951902
ENST00000565797	-1.215576	POLR3D	1.2037104	PLAU	-1.68325923
LINC00087	2.40802667	CARD18	1.20665364	DKK1	-1.85644209
OSER1-AS1	1.94942429	SORL1	-1.5949261	DHCR7	1.387017042
ENST00000528497	-1.5022894	BTG1	1.54531401	STX5	1.222643411
SNHG7	1.26453778	CCL2	-1.639896	NF2	-1.24080712
FAM155A-IT1	2.48184995	CBX4	1.22578309	CDCA7	-1.45629578
MCM3AP	1.29368161	PPP1R15A	2.30120411	FILIP1L	-1.47074715
LOC101929340	-1.8149866	DYRK1B	1.26129406	PFN2	-1.2359365
IDH1-AS1	1.24930483	TMEM2	-1.2314209	SOD3	1.476986997
LINC01444	-1.7138095	HMGA2	-1.9958206	RWDD2A	1.334785097
lnc-RP11-17M16.1.1-1	1.56727317	ERCC6L	-1.5542503	SEMA3C	-1.27409457
BTG1	1.80931627	GPRASP1	-1.2070056	WDHD1	-1.43092727
ENST00000556144	2.00396909	PAQR6	1.40146785	DNAJB9	2.13936258
ENST00000425771	1.46199443	RRAGC	1.32101836	C14orf1	1.328146976
lnc-TBC1D12-1	-2.8554959	TXNIP	1.86886064	LAT2	-1.89581474
lnc-TCL1B-2	2.60129601	BIRC3	-1.8085436	TST	1.479744697
lnc-YIF1A-6	1.77040939	FADS2	1.49990123	OBSL1	1.378537317
CCNT2-AS1	2.16926885	MYO7A	1.48162415	HMGCR	1.882679139
lnc-MFSD6-1	-1.241593	CDK2	-1.4435573	ACAT2	1.772368514
lnc-SHISA4-1	2.62102229	IDI1	1.93336897	RFTN1	-1.30786086
ENST00000439105	1.37684166	DNM1P46	2.31652379	DNHD1	2.255140049
TSC22D2	-1.2860422	LSS	1.5524667	GOLGA5	1.468467678
lnc-CLCN6-1	1.70162087	FDPS	1.64375629	FAM76A	1.214851766
lnc-MFSD9-4	3.02982147	KLHDC7B	2.52055913	NFIL3	1.834511456
lnc-CETP-1	2.72861176	SH3RF2	-1.5818393	U2AF1L4	1.332855607
PMP22	-1.4221538	CYP51A1	1.30753076	STARD4	1.647013649
SFRP1	-1.7372767	RTKN2	-1.2327059	NEURL3	1.548162472
C3	-2.0167746	CD86	2.73301857	MNS1	-1.49088668

TMEM2 in pancreatic cancer: biomarker analysis & NSC777201 drug potential

Gene	Value	Gene	Value	Gene	Value
ACOX2	-2.8101865	IFRD1	1.23520001	MAF1	1.295193232
SNPH	1.45254887	HS1BP3	1.50422758	ZFAND2A	1.34105766
OSCP1	1.53909661	FAM111A	-1.25812	IFNL1	3.249302712
DDIT4	2.0073865	VAT1	1.55733465	G6PD	1.522362761
MYPN	-1.3384496	IRS2	1.59474623	MAGEH1	1.663407733
SLC29A2	1.45502113	SERPINE1	-1.2225491	STARD13	-1.2334489
MVK	1.93855449	ENST00000526512	1.689252	SYNPO	-1.26494352
MSMO1	1.69899739	AK027667	-1.6133828	ATF3	3.872722344
ZNF185	-1.5804366	PXN	-1.4244505	SESN2	2.968848899
AKAP12	-1.2214691	TMEM97	1.53282605	KLHL35	1.289613038
LYNX1	1.73133884	FADS1	1.3553134	ANLN	-1.2530578
SMIM14	1.2336414	THC2525241	-1.2366098	E2F8	-1.23252804
SHISA4	1.28305534	RHBDL2	-2.5164811	MYEOV	-2.07111008
TM7SF2	2.50314166	ZNF365	-1.3469716	MIS18BP1	-4.33718236
LARP6	1.22630628	FAM129A	2.33989935	LINC00346	1.708492524
GINS2	-1.3051251	ARMCX3	1.26582292	MCM4	-1.69221335
HSD17B7	2.01814773	CSTF3	-1.3048441	CMIP	-1.28268343
KLF2	1.4990265	BET1	1.36098437	FUZ	2.374916743
DNASE2	1.45211091	NUPR1	3.24090783	RPS6KA5	1.372420262
XBP1	1.42792858	TMEM150A	1.33917302	ADAM19	-1.74876399
HMOX1	3.76729004	ADAM8	-1.8207219	GAL	-1.21358028
ATF4	1.20778676	ENST00000433309	1.53305118	BMF	2.151281537
PTX3	-2.5747841	KRT80	-2.1482474	BBC3	1.429481726
CAV2	-1.2542748	FAM212B	1.33862076	MFI2	-1.20538235
CNN1	-1.4201668	ATF3	4.51451938	ZNF512	-1.3054448
CTH	1.86834016	SLC16A14	-1.6550554	HAS3	-2.52095794
CLSPN	-1.2828862	PRELID2	-1.3782808	FKBP1A	-1.20712128
LAYN	-1.4236795	MKI67	-1.3566609	MTHFR	1.434812324
HELLS	-1.525508	TCF19	-1.2936694	PRSS22	-1.39917088
FICD	1.62073518	NT5E	-1.8404676	FXR2	1.906969073
PCK2	1.89444996	LPCAT2	-1.2977501	TARDBP	-1.38359503
CLCN7	1.35192101	RAP1GAP	2.59503177	CREBRF	1.587056578
TBC1D17	1.36789469	TRAPPC6A	1.99619138	SNAI3-AS1	2.985599542
HES6	1.52146643	NEU1	1.4825559	MXD1	1.336231394
MANF	1.21869331	CDC25A	-1.8438413	E2F2	-1.29029377
COL13A1	-2.0984227	TGFB2	-1.5456081	IFNL2	2.880231904
SLC29A1	-1.230821	PCYT2	1.74131858	CEBPB	1.223685893
CAV1	-1.2731324	MAPK13	-1.4338421	IFFO2	-1.30145867
UAP1L1	1.63305031	RAB39B	1.47697774	SREBF2	1.264422895
EIF2AK3	1.68504072	GPR126	-1.2606729	TNFAIP2	-1.6065168
SLC16A2	-1.2224534	TMA7	-4.3453436	SLC35F3	-1.30240786
PRPH	1.64208819	VCL	-1.6559542	MXD4	1.500998787
SIPA1L2	1.41905945	GABARAPL1	1.37440919	SH3BP5L	1.273969428
MED18	-1.9144543	KLHL24	1.55913925	NFE2L3	-1.48422965
GOLGA2P5	1.20359259	H19	-1.501911	CDKN1C	1.531094616
WIPI1	1.71135456	GJA1	-1.2274376	SPOCD1	-2.81739299
RDM1	-1.759908	PPARA	1.35211057	MYBL1	-1.41485561
RFC3	-1.2204591	HMGCS1	2.5160713	P2RX5	-1.24970808
MKNK2	1.37271742	ENC1	-2.0228836	ZNF107	-1.23207444

TMEM2 in pancreatic cancer: biomarker analysis & NSC777201 drug potential

FAM134A	1.32557491	WFDC21P	2.09941739	LOC284513	-1.27440651
ATP6V1E2	1.40298846	TRNP1	-1.666595	DKFZP564C152	1.598063021
TIPARP	1.42345345	LRRC73	1.30379357	MCM10	-1.38886525
COL7A1	-1.2796141	TMEM191B	1.20353963	MPV17L	-1.21610138
GNPDA1	1.28983526	METTL12	1.21828004	lnc-SERPINC1-1	1.540820233
PDLIM7	-1.2543542	TMEM198	2.02818898	LOC101927751	-1.52599579
GCLC	1.64743743	MMACHC	-1.2219689	MT1F	2.620129078
ASNS	1.30616299	JAM3	-1.4105086	BCL2A1	-2.50956838
SQLE	1.46464791	PHLDA1	-1.6460961	MVD	3.090773607
RAB33A	2.17240884	TGM2	-2.2396187	ATG7	-1.20849705
EPHA2	-1.5597151	MKNK2	1.75168465	HSPA5	1.319652654
IGF2	-1.284541	HMBOX1	3.10521185		
PLEK2	-1.3252696	DIDO1	-1.333093		
C8orf60	-1.4285523	GABARAPL1	1.20407627		
LINC00087	1.99532205	GPATCH2L	-8.4714465		
AKAP12	-1.395977	KIAA1462	-1.2066192		
SLCO4C1	3.83982388	SH2D3C	2.6683409		
FOXQ1	-1.8744062	ANGPTL4	-2.0332006		
HEG1	-1.6016776	RNF207	-1.2848771		
JMY	1.85285807	COL1A1	-2.1448519		
ITGA2	-1.8934376	ATF6B	1.21196305		
ERICH2	2.37501487	PLAU	-1.5152833		
ELFN2	-1.6363074	RHOB	1.32244839		
ARHGEF37	1.38718491	AB209400	-2.1737168		
FOXP4-AS1	-1.6585327	LONP1	1.38764415		
A_32_P230825	1.85578539	RNF207	-1.2699389		
GAS5	1.80713723	BQ934349	-1.2074767		
FHOD3	-1.8404391	HES6	1.25156886		
SC5D	1.69662496	ENST00000581935	-1.4137898		
RHBDL2	-2.8787798	A_33_P3324552	2.0625647		
LPIN1	1.46250196	JUND	1.45596025		
PPP1R1C	-1.5629728	SH3BGR	1.61851403		
ID2	1.24723173	FASN	2.21967256		
TSPAN15	-1.28635	CDK2AP2	1.29744333		
C11orf96	3.09633032	CXCL1	-1.5577778		
ALG10B	-1.230826	LINC00173	-1.4978892		
FDPSP2	1.55835559	HSD17B12	1.76882947		
MMS22L	-1.4288483	LAMB3	-1.5603719		
ATF3	3.88052861	GINS1	-1.2468923		
AP5Z1	1.2697282	NEXN	-1.9619152		
PDLIM7	-1.262431	PRDM8	-1.2695531		
MID1IP1	1.3489739	ENST00000443279	1.37347563		
JMY	1.83777188	THC2685534	1.26796611		
INSIG1	2.20635322	ETV2	1.33934361		
HSD17B7	2.02900773	RPS4X	-1.9523427		
CCDC149	1.94941034	PLCE1	-1.2435921		
BET1L	1.23915974	CABP7	-1.5682147		
ZNF419	1.55010457	FAM213A	1.56836442		
SLC25A36	1.21852491	ENDOV	1.79595583		

|			
HIST2H2BF	1.26369032	USP36	1.3503221
RAB17	1.49867079	YIF1A	1.33814759
A_33_P3232544	1.80335881	TGFB2-AS1	-1.8357873
RAMP1	1.52305877	MMAB	1.90069057
ASS1	1.87139271	MT1H	5.3846792
SPSB3	1.26625713	LY9	2.5824098
NSDHL	1.31766372	LURAP1L	1.38912583
TSC22D3	3.34167796	ATP9A	1.41351387
PXDN	-1.4447263	LOC729970	1.94230321
FRMD5	-1.4264083	CHAC1	2.95164457
XRCC2	-1.5181799	CHAC1	2.70410701
GFPT1	1.26705061	UHRF1	-1.2616279
C17orf59	1.65492579	STARD13	-1.3057901
BEX2	3.12393642	THSD4	-1.4540368
CCNE2	-1.5707683	ABCC6	-1.3063285
A_33_P3247678	-1.5867694	SNAI3-AS1	1.92580627
SLC33A1	1.23647002	LAMA4	-2.4851629
VIMP	1.42373289	PCYT2	1.66401447
GADD45G	1.55209115	SYNPO	-1.4277057
GGT5	-1.4620565	CYS1	1.33963279
MIIP	1.27910468	RHOB	1.6265443
HELLS	-1.2437358	UBE3A	-2.7419847
HAPLN3	-1.5250778	SLC6A9	1.51699477
ENST00000610439	-1.4891098	A_33_P3406090	2.35604283
CCDC114	1.26156452	UBASH3B	-1.4228949
HES6	1.47707764	ADAL	-1.407594
MIR4435-1HG	-1.2828727	OXTR	-2.9212095
FAM111B	-1.7631042	ACLY	1.33218597
PXDN	-1.3345993	ANKRD36B	-1.408806
YIPF2	1.40420012	AMDHD2	1.5121163
HID1	2.37534028	CHORDC1	-1.2273439
HSD17B7	1.99276963	VSTM1	-1.6699898
PCYT2	1.47972711	ERCC8	-1.2319687
A_33_P3278684	2.75231334	A1BG	1.20959607
THY1	-1.353997	MIR146A	-2.3947785
RPS29	1.28878959	ISOC2	1.55979523
CLDN3	2.16199989	RNU4ATAC	2.25168189
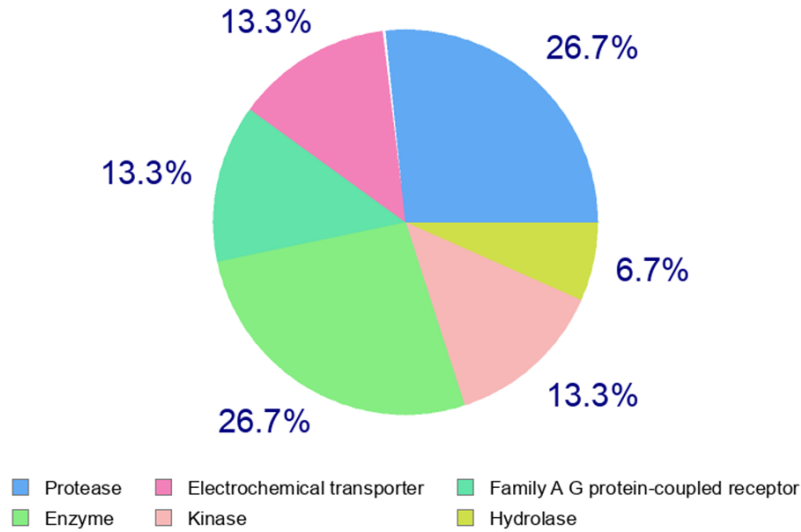
Figure S5. Predictive NSC777201 targets. Different enzymes, molecules or receptors, such as kinases, protease etc., that our drug can targets shown in pie chart with percentage.
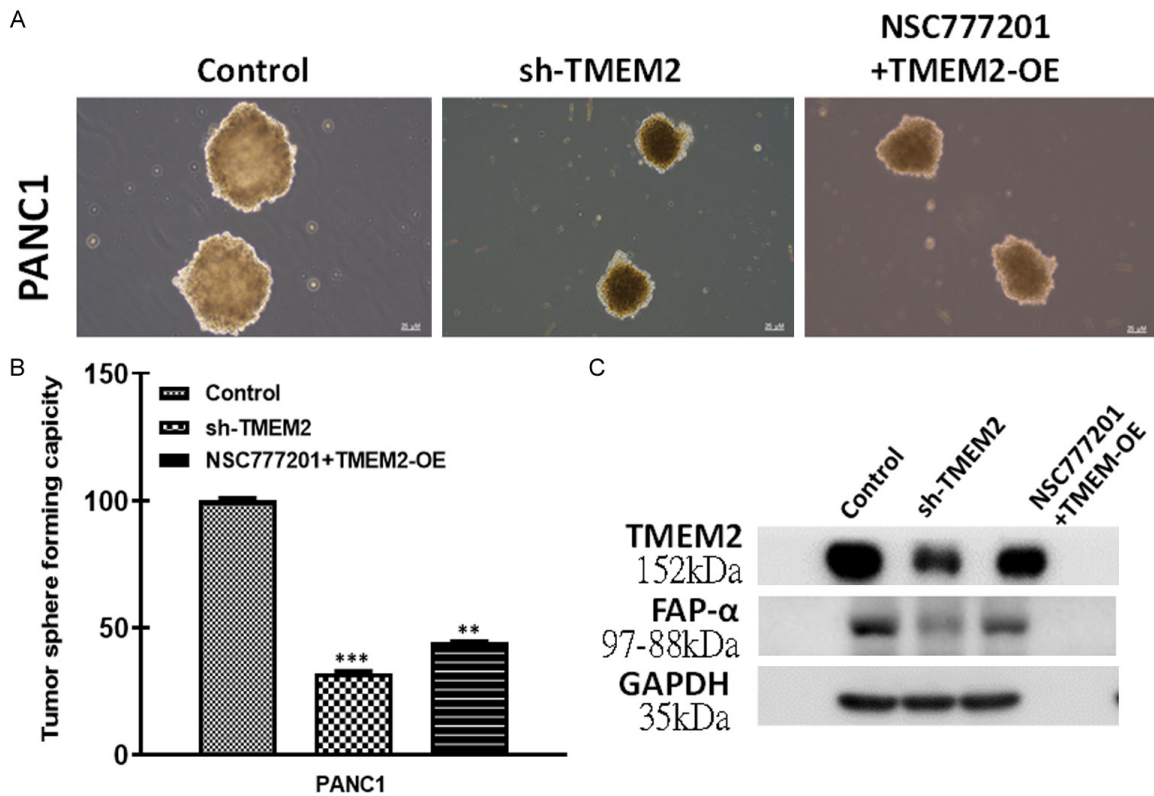

Figure S6. NSC777201 played its anti-PAAD effect through inhibiting TMEM2 expression on Panc1 cells. TMEM2 stably over-expressed (TMEM-OE) or inhibited (sh-TMEM2) in Panc1 cells were achived through transfection of lentivirus, and the expression efficiency was verified by WB. The control and TMEM2 stably overexpressed Panc1 cells were treated with NSC777201 or control to show rescue effect. A, B. Tumor sphere formation capacity were respectively determined by the sphere-forming experiments. C. The expression of TMEM2 proteins was verified using the WB experiment. GAPDH served as the loading control.